



1 Evaluating a fire smoke simulation  
2 algorithm in the National Air Quality  
3 Forecast Capability (NAQFC) by using  
4 multiple observation data sets during the  
5 Southeast Nexus (SENEX) field campaign

6 Li Pan<sup>1,2</sup>, Hyun Cheol Kim<sup>1,2</sup>, Pius Lee<sup>1</sup>, Rick Saylor<sup>3</sup>, YouHua Tang<sup>1,2</sup>, Daniel Tong<sup>1,2</sup>, Barry Baker<sup>1,2</sup>,  
7 Shobha Kondragunta<sup>4</sup>, Chuanyu Xu<sup>5</sup>, Mark G. Ruminski<sup>4</sup>, Weiwei Chen<sup>1,6</sup>, Jeff Mcqueen<sup>7</sup> and Ivanka  
8 Stajner<sup>8</sup>

9 <sup>1</sup> NOAA/OAR/Air Resources Laboratory, College Park, MD 20740, USA

10 <sup>2</sup> UMD/Cooperative Institute for Climate and Satellites, College Park, MD 20740, USA

11 <sup>3</sup> NOAA/OAR/ARL/Atmospheric Turbulence and Diffusion Division, Oak Ridge, TN 37830, USA

12 <sup>4</sup> NOAA/NESDIS, College Park, MD 20740, USA

13 <sup>5</sup> I. M. Systems Group at NOAA, College Park, MD 20740, USA

14 <sup>6</sup> Northeast Institutes of Geography and Agroecology, Chinese Academy of Sciences, Changchun 130102,  
15 P. R. China

16 <sup>7</sup> NOAA/NCEP/Environmental Modeling Center, College Park, MD 20740, USA

17 <sup>8</sup> NOAA/NWS Office of Science and Technology Integration, Silver Spring, MD 20910, USA

18  
19 Correspondence to: Li.Pan@noaa.gov  
20  
21  
22  
23  
24



## 25 **Abstract**

26 Multiple observation data sets: Interagency Monitoring of Protected Visual Environments  
27 (IMPROVE) network data, Automated Smoke Detection and Tracking Algorithm (ASDTA), Hazard  
28 Mapping System (HMS) smoke plume shapefiles and aircraft acetonitrile (CH<sub>3</sub>CN) measurements from  
29 the NOAA Southeast Nexus (SENEX) field campaign are used to evaluate the HMS-BlueSky-SMOKE-  
30 CMAQ fire emissions and smoke plume prediction system. A similar configuration is used in the US  
31 National Air Quality Forecasting Capability (NAQFC). The system was found to capture most of the  
32 observed fire signals. Usage of HMS-detected fire hotspots and smoke plume information were valuable  
33 for both deriving fire emissions and forecast evaluation. This study also helped identified that the  
34 operational NAQFC did not include fire contributions through lateral boundary conditions resulting in  
35 significant simulation uncertainties. In this study we focused both on system evaluation and evaluation  
36 methods. We discussed how to use observational data correctly to filter out fire signals and  
37 synergistically use multiple data sets. We also addressed the limitations of each of the observation data  
38 sets and evaluation methods.

## 39 **Introduction**

40 Wildfires and agricultural/prescribed burns are common in North America all year round, but  
41 predominantly occur during the spring and summer months (Wiedinmyer et al., 2006). These fires pose  
42 a significant risk to air quality and human health (Delfino et al., 2009; Rappold et al., 2011; Dreessen et  
43 al., 2016; Wotawa and Trainer 2000; Sapkota et al., 2005; Jaffe et al., 2013; Johnston et al., 2012). Since  
44 January 2015, smoke emissions from fires have been included in the National Air Quality Forecasting  
45 Capability (NAQFC) daily PM<sub>2.5</sub> operational forecast (Lee et al., 2017). The NAQFC fire simulation consists  
46 of: the NOAA National Environmental and Satellite Data and Information Service (NESDIS) Hazard  
47 Mapping System (HMS) fire detection algorithm, the U.S. Forest Service (USFS) BlueSky-fire emissions



48 estimation algorithm, the U.S. EPA Sparse Matrix operator Kernel Emission (SMOKE) applied for fire  
49 plume rise calculations, the NOAA National Weather Service (NWS) North American Multi-scale Model  
50 (NAM) for meteorological prediction and the U.S. EPA Community Multi-scale Air Quality Model (CMAQ)  
51 for chemical transport and transformation. In contrast to most anthropogenic emissions, smoke  
52 emissions from fires are largely uncontrolled, transient and unpredictable. Consequently, it is a  
53 challenge for air quality forecasting systems such as NAQFC to describe fire emissions and their impact  
54 on air quality (Pavlovic et al., 2016; Lee et al., 2017; Huang et al., 2017).

55 Southeast Nexus (SENEX) was a NOAA field study conducted in the Southeast U.S. in June and  
56 July 2013 (Warneke et al., 2016). This field experiment investigated the interactions between natural  
57 and anthropogenic emissions and their impact on air quality and climate change (Xu et al., 2016;  
58 Neuman et al., 2016). In this work, we used the SENEX dataset to evaluate the HMS-BlueSky-SMOKE-  
59 CMAQ fire simulations during the campaign period.

60 Two simulations were performed: one with and one without smoke emissions from fires during  
61 the SENEX field campaign. Due to the large uncertainties in the estimates of fire emissions and smoke  
62 simulations (Baker et al., 2016; Davis et al., 2015; Drury et al., 2014), the first step of the evaluation  
63 focused on the fire signal capturing capability of the system. Differences between the two simulations  
64 represented the impact of the smoke emissions from fires on the CMAQ model results. Observations  
65 from various sources were utilized in this analysis: (i) ground observations (Interagency Monitoring of  
66 Protected Visual Environments (IMPROVE)), (ii) satellite retrievals (Automated Smoke Detection and  
67 Tracking Algorithm (ASDTA) and HMS smoke plume shape), and (iii) aircraft measurements (SENEX  
68 campaign). Fire signals predicted by the modeling system were directly compared to these observations.  
69 Several criteria have been used to rank efficacy of the observation systems for fire induced pollution  
70 plumes.



## 71 **Methodology**

72 In this section we introduce the NAQFC fire modeling system used in the study. Uncertainties  
73 and limitations in the various modeling components of the system are discussed. Fig. 1 illustrates the  
74 schematics of the system. There are four processing steps:

### 75 **HMS (Hazard Mapping System)**

76 The NOAA NESDIS HMS is a fire smoke detection system based on satellite retrievals. The  
77 satellite constellation used comprised of 2 Geostationary Operational Environmental Satellite (GOES-10  
78 and GOES-12) and 5 polar orbiting satellites (MODIS (Moderate-resolution Imaging Spectroradiometer))  
79 -- Terra and Aqua, AVHRR (Advanced Very High Resolution Radiometer) 15/17/18). HMS detects  
80 wildland fire locations and analyzes their sizes, starting times and durations (Ruminski et al., 2008;  
81 Schroeder et al., 2008; Ruminski and Kondragunta 2006).

82 HMS first processes satellite data by using automated algorithms for each of satellite platforms  
83 to detect fire locations (Justice et al., 2002; Giglio et al., 2003; Prins and Menzel 1992; Li et al., 2000),  
84 which is then manually analyzed by analysts to eliminate false detections and/or add missed fire  
85 hotspots. The size of the fire is represented by the number of detecting pixels corresponding to the  
86 nominal resolution of MODIS or AVHRR data. Fire starting times and durations are estimated from close  
87 inspection of the visible band satellite imagery. A bookkeeping file is generated at the end of this  
88 detection step, named "hms.txt". It includes all the thermal signal hotspots detected by the  
89 aforementioned 7 satellites. During the analyst quality control step, detected potential fire hotspots  
90 lacking visible smoke in the retrieval's RGB real-color imagery are removed resulting in a reduced fire  
91 hotspot file called either "hmshysplit.prelim.txt" or "hmshysplit.txt" to be input into the BlueSky  
92 processing step.



93 In general, “hmsysplit.prelim.txt” and “hmsysplit.txt” are very similar, and “hmsysplit.txt” is  
94 created later than “hmsysplit.prelim.txt” (Fig. 1). But the differences between “hmx.txt” and  
95 “hmsysplit.txt” (“hmsysplit.prelim.txt”) can be rather substantial. The reasons for differences are: 1)  
96 many detected fires do not produce detectable smoke; 2) some fires/hotspots are detected only at  
97 night, when smoke detection is not possible; 3) smoke emission RGB imageries are obscured by clouds  
98 thus not detected by the analyst. Therefore, smoke emission occurrence provided by the HMS is a  
99 conservative estimate of fire emissions.

100 By using multiple satellites the likelihood of detecting fires in HMS is robust. However, when the  
101 fire geographical size is small the HMS detection accuracy dramatically decreases (Zhang et al., 2011; Hu  
102 et al., 2016). Other limitations of the HMS fire detections include ineffective retrievals at nighttime and  
103 under cloud cover.

## 104 **BlueSky**

105 BlueSky, developed by the USFS (US Forest Service), is a modeling framework to simulate smoke  
106 impacts on regional air quality (Larkin et al., 2009; Strand et al., 2012). In this study, BlueSky acted as a  
107 fire emission model to provide input for SMOKE (Herron-Thorpe et al., 2014; Baker et al., 2016). BlueSky  
108 calculates fire emission based on HMS-derived locations (Fig. 1).

109 Fire geographical extent is reflected by the number of nearby fire pixels detected by satellites in  
110 a 12 km resolution CMAQ model grid. Fire pixels are converted to fire burning areas in BlueSky based on  
111 the assumption that each fire pixel has a size of 1 km<sup>2</sup> and 10% of its area can be considered as burn-  
112 active (Rolph et al., 2009). All fire pixels in a 12 km grid square are aggregated. BlueSky uses the  
113 following to estimate biomass availability: fuel loading map is from the US National Fire Danger Rating  
114 System (NFDRS) for the Conterminous US (CONUS) with the exception in western US where the HARDY  
115 set is used (Hardy and Hardy 2007). BlueSky uses Emissions Production Model (EPM) (Sandberg and



116 Peterson 1984), a simple version of CONSUME, to calculate fuel actually burned -- the so-called  
117 consumption sums. Finally, EPM is also used in BlueSky to calculate the fire emission hourly rate per  
118 grid-cell. BlueSky outputs CO, CO<sub>2</sub>, CH<sub>4</sub>, non-methane hydrocarbons (NMHC), total PM, PM<sub>2.5</sub>, PM<sub>10</sub> and  
119 heat flux (Fig. 1).

120 BlueSky does not iteratively recalculate fire duration according to the modeled diminishing fuel  
121 loading or the modeled fire behavior. In the aggregation process, when there is more than one HMS  
122 point in a grid cell which have different durations, all points in that grid cell would be assigned the  
123 largest duration in all points. For an example, if there were 3 HMS points that had durations of 10, 10  
124 and 24 hours, the aggregation would include 3 points (representing 3 km<sup>2</sup>) assigned with 24 hour  
125 duration to all of the 3 HMS points.

126 HMS has no information about fuel loading. BlueSky uses a default fuel loading climatology over  
127 the eastern US. BlueSky uses an idealized diurnal profile for fire emissions. Uncertainties in fire sizes,  
128 fuel loading and fire emissions rate lead to large uncertainties in wildland smoke emissions (Knorr et al.,  
129 2012; Drury et al., 2014; Davis et al., 2015).

## 130 **SMOKE**

131 In SMOKE (Sparse Matrix Operator Kernel Emission), the BlueSky fire emissions data in a  
132 longitude-latitude map projection are converted to CMAQ ready emission gridded files (Fig. 1). Fire  
133 smoke plume rise is calculated using formulas by Briggs. The heat flux from BlueSky and NAM  
134 meteorological state variables are used as input (Erbrink 1994). The Briggs' algorithm calculates plume  
135 top and plume bottom, between plume top and bottom the emission fraction is calculated layer by layer  
136 assuming a linear distribution of flux strength in atmospheric pressure. For model layers below the  
137 plume bottom the emission fraction is assumed to be entirely in the smoldering condition as a function  
138 of the fire burning area.



139 We adopted a speciation cross-reference map to match BlueSky chemical species to that in  
140 CMAQ using the U.S. EPA Source Classification Codes (SCCs) for forest Wildfires  
141 (<https://ofmpub.epa.gov/scsearch/docs/SCC-IntroToSCCs.pdf>). The life-span of fire is based on the HMS  
142 detected fire starting time and duration. During fire burning hours a constant emission rate is assumed.  
143 This constant burn-rate has been shown to be a crude estimate (Saide et al., 2015; Alvarado et al.,  
144 2015). Other uncertainties include plume rise (Sofiev et al., 2012; Urbanski et al., 2014; Achtemeier et  
145 al., 2011) and fire-weather (fire influencing local weather).

#### 146 **CMAQ**

147 The CMAQ version 4.7.1 was used. We chose the CB05 gas phase chemical mechanism (Yarwood  
148 et al., 2005) and the AERO5 aerosol module (Carlton et al., 2010). Anthropogenic emissions were based  
149 on the U.S. EPA 2005 National Emission Inventory (NEI) projected to 2013 (Pan et al., 2014), Biogenic  
150 emissions (BEIS 3.14) were calculated in-line inside CMAQ.

#### 151 **Simulations**

152 The NAM provided meteorology fields to drive CMAQ (Chai et al., 2013). NAM meteorology is  
153 evaluated daily and results (BIAS and RMSE etc.) are posted on:  
154 "<http://www.emc.ncep.noaa.gov/mmb/mmbpll/mmbverif/>". The simulation domain is shown in Fig. 1.  
155 It includes two domains: (i) a 12km domain covering the Continental U.S. (CONUS); and (ii) a 4km  
156 domain covering the Southeast U. S. where the majority of SENEX measurements occurred. Lateral  
157 boundary conditions (LBC) used in the smaller SENEX domain simulation were extracted from that from  
158 the CONUS simulations. Four scenarios were simulated: CONUS with fire emissions, CONUS without fire  
159 emissions, SENEX with fire emissions and SENEX without fire emissions.

160 There were several differences in system configuration between the NAQFC fire smoke  
161 forecasting and the "with-fire" simulation in this study. For models, the BlueSky versions used in NAQFC



162 and that in this study are v3.5.1 and v2.5, respectively; CMAQ versions used in NAQFC and in this study  
163 are v5.0.2 and v4.7.1, respectively. For simulations, current fire smoke forecasting in the NAQFC  
164 includes two runs: the analysis and the forecast (Huang et al. 2018 (manuscript in preparation)). The  
165 analysis run is a 24-hour retrospective simulation to rerun yesterday's fire emissions using yesterday's  
166 meteorology providing an initial condition for today's forecast. The forecast run is a 48-hour forecasting  
167 simulation to run yesterday's fire emissions to be projected as continued fires had their burn duration  
168 were more than 24 hours. The "with-fire" simulation in this study is exactly identical to the analysis run  
169 in NAQFC.

## 170 **Evaluations**

171 Carbon monoxide (CO) has a relatively long life time in the air and is commonly associated with  
172 biomass burning. CO was used as a fire tracer in the prediction. The CO difference ( $\Delta\text{CO}$ ) between  
173 CMAQ simulations with and without fire emissions was used as the indicator of fire influence. For  
174 additional observations we used: potassium (K) collected at the IMPROVE (Interagency Monitoring of  
175 Protected Visual Environments) sites within the SENEX domain; acetonitrile ( $\text{CH}_3\text{CN}$ ) measured from the  
176 SENEX campaign flights; and fire plume shape detected by the HMS analysis as real fire signals. The  
177 enhancement in  $\Delta\text{CO}$  concentration due to fire was directly compared with those signals. At the same  
178 time,  $\Delta\text{AOD}$  (Aerosol Optical Depth) from CMAQ ("with-fire" simulated concentration minus that with  
179 "without-fire") was also used as fire indicator when compared with smoke masks given by the ASDTA  
180 (Automated Smoke Detection and Tracking Algorithm).

181 In this study, we have focused on evaluations subject to the large uncertainties of the underlying  
182 physical processes of smoke emissions from fires and its transport. In each modeling step in HMS,  
183 BlueSky, SMOKE and CMAQ, the modeling system accrues uncertainties. Such uncertainties were likely  
184 cumulative and might lead to larger error in succeeding components (Wiedinmyer et al., 2011). For an



185 example, heat flux from BlueSky influenced plume rise height in SMOKE and consequently influenced  
186 plume transport in CMAQ. It is also noteworthy that when we compared modeled  $\Delta\text{CO}$  against  
187 measured K or  $\text{CH}_3\text{CN}$ , the objective was to search for enhancement signals resulting from fires but it  
188 was not aiming to account for proportional concentration changes in the tracers. Attempting to account  
189 for CMAQ simulation uncertainties in surface ozone and particulate matter as a function of smoke  
190 emissions from fires was difficult. Neither was it the objective of this study. Rather, the purpose of this  
191 study is to focus on analyzing the capability of the HMS-BlueSky-SMOKE-CMAQ modeling system to  
192 capture the timing of fire signals.

193 The SENEX campaign occurred in June and July and our model simulations were from June 10 to  
194 July 20, 2013. Throughout the campaign we used all available observation datasets including ground-,  
195 air- and satellite-based acquired data. Each dataset had its unique characteristics and linking them  
196 together gave an overall evaluation. At the same time, in each dataset our evaluations included as many  
197 as possible observed fire cases. Both well-predicted and poorly-predicted cases are presented to  
198 illustrate potential reasons responsible for the modeling system's behavior.

## 199 **Results and Discussions**

### 200 **Observed CO versus modeled CO in SENEX**

201 Table 1 lists observed and modeled CO vertical profiles for the “with-fire” and “without-fire”  
202 cases during the SENEX campaign. Observed CO concentrations between the surface and 7 km AGL  
203 (Altitude above Ground Level) in the SENEX domain area remained greater than 100 ppb during all 40  
204 days of the campaign. The highest CO concentrations were measured closer to the surface. The  
205 maximum measured CO concentration of 1277 ppb was observed during a flight on July 03 at an ASL  
206 (Altitude above Sea Level) of 974 m. In this flight strong fire signals were observed but the fire  
207 simulation system missed those signals as discussed below.



208 CO concentrations were underestimated by the model in almost all cases even when the model  
209 captured CO contribution from fire emissions spatio-temporarily. Mean  $\Delta\text{CO}$  in each height interval was  
210 usually above 1.5 ppb but less than 2.0 ppb. Fig. 2a exhibits the contribution of total CO emissions from  
211 fires which occurred inside the SENEX domain over the simulation period. The maximum CO emissions  
212 contribution from fires was about 3% during the campaign. In most of those days fire emission  
213 contributions in SENEX were less than 1%. The averaged contribution during those 40 days was 0.7%.  
214 Fig. 2b exhibits the contribution of CO flowing into the SENEX domain from its boundary caused by fire  
215 outside the SENEX domain but inside the CONUS domain (Fig. 1). The averaged fire contribution to CO  
216 from outside the SENEX domain was 0.67%. CO influenced by fire emission in June is greater than that in  
217 July.

218 During the field experiment the general lack of large fires made evaluation of modeled fire  
219 signature difficult since it was easier to capture large fire signals than the smaller fires. We postulated  
220 that a clear fire signal simulated in the HMS-BlueSky-SMOKE-CMAQ system could be indicated by  $\Delta\text{CO}$   
221 significantly larger than its temporal averages resulted by fires originated from inside and/or outside the  
222 SENEX domain. For an example, if a clear fire signal between 500 m and 1000 m AGL is represented by  
223  $\Delta\text{CO}$  in a model simulation and the concentration of  $\Delta\text{CO}$  is above 2.0 ppb, based on the average CO  
224 concentration of about 150 ppb as well as on with SENEX domain and outside of SENEX domain fire  
225 contributions of  $(150 \cdot (0.007 + 0.0067)) = 2.0$ .

226 Figure 3 displays the simulated  $\Delta\text{CO}$  extracted along a SENEX flight path. The modeled  
227 concentration showed that the fire impacts on SENEX were not negligible perspective despite a lack of  
228 larger fire events as shown in Fig. 2a and 2b during the SENEX campaign period. That confirmed the  
229 importance of evaluating the fire simulation system in an air quality model. Unless a model is able to  
230 predict fire signals correctly it is useless for modelers to discuss fire effects on chemical composition of



231 the atmosphere. A detail of how our model caught or missed or falsely predicted fire signals during the  
232 SENEX campaign and a comparison of  $\Delta\text{CO}$  versus  $\text{CH}_3\text{CN}$  will be discussed in the follow discussion.

### 233 **IMPROVE**

234 The Interagency Monitoring of Protected Visual Environments (IMPROVE) is a long term air  
235 visibility monitoring program initiated in 1985 (<http://vista.cira.colostate.edu/Improve/data-page>). It  
236 provides 24-h integrated particulate matter (PM) speciation measurements every third day (Malm et al.,  
237 2004; Eatough et al., 1996). The IMPROVE dataset was chosen for this analysis because it included K  
238 (potassium), OC (organic carbon) and EC (elemental carbon), important fire tracers. IMPROVE monitors  
239 are ground observation sites likely influenced by nearby fire sources.

240 There were 14 IMPROVE sites in the SENEX domain (Fig. 4). Potential fire signals were identified  
241 by using CMAQ modeled  $\Delta\text{CO}$  and IMPROVE observed K. However, in addition to fires K has multiple  
242 sources such as soil, sea salt and industry. Co-incidentally fires should also produce enhanced EC and OC  
243 concentrations, a fire signal should reflect above-average values for EC, OC, and K. EC, OC and K  
244 observations that were 20% above their temporal averages during the SENEX campaign were used as a  
245 predictor for fire event identification. Meanwhile, co-measured  $\text{NO}_3^-$  and  $\text{SO}_4^{2-}$  concentrations 50%  
246 below their respective temporal averages was used to screen out data with industrial influences. Lastly,  
247 a third predictor was employed so that concentrations of other soil components besides K should be  
248 below their temporal average to eliminate conditions of spikes in K concentration due to dust. With  
249 these three criteria the IMPROVE data was screened for fire events (See Table 2).

250 Five fire events were observed at four IMPROVE sites. Table 2 lists measured EC, OC,  $\text{NO}_3^-$ , K, soil  
251 and  $\text{SO}_4^{2-}$  concentrations ( $\mu\text{g m}^{-3}$ ) and their ratios to averages. BC versus OC and K versus BC ratios were  
252 also calculated and listed in Tab. 2 to illustrate the application of our criteria. We found that except for  
253 monitor BRIS, all other sites (COHU, MACA and GRSM) had BC/OC and K/BC ratios comparable to the



254 ratios of the same quantities due to biomass burning reported by other researchers (Reid et al., 2005;  
255 DeBell et al., 2004). BRIS is a coastal site likely influenced by sea salts (Fig. 4).

256 For the four identified fire cases, we plotted  $\Delta\text{CO}$  as a modeled fire tracer around the IMPROVE  
257 sites. Our model simulation reproduced fire signals on June 21 at COHU and GRSM and on June 24 at  
258 MACA. We used the June 24 MACA case as an example (see Fig. 4) – closed black circles represent the  
259 detected fire locations; closed triangles represents IMPROVE sites, and  $\Delta\text{CO}$  values above 2.0 ppb were  
260 shown. On June 24, 2013, detected fire spots were outside the SENEX domain, but SSW wind blew  
261 smoke plumes into the SENEX domain and affected modeled CO in MACA. Modeled  $\Delta\text{CO}$  in MACA was 5  
262 ppb.

263 Another IMPROVE site located upwind of MACA, CADI, was also potentially under the influence  
264 of that fire event; however, data from CADI on June 24 did not indicate a fire influence, possibly due to  
265 the frequency of IMPROVE sampling that eluded measurement or that the smoke plume was  
266 transported above the surface in disagreement with what was modeled. Within the four fire cases  
267 identified by the IMPROVE data during SENEX (Tab. 2), the model successfully captured three out of four  
268 events. The model missed fire signal on July 3 at MACA. The model missed the fire signal on July 3 at  
269 MACA. The following section is dedicated for the July 3 SENEX flight.

## 270 **Plume Spatial Coverage**

271 HMS determines fire hotspot locations associated with smoke and upon incorporating the  
272 smoke plume shape information from visible satellite images. HMS provides smoke plume shapefiles  
273 over much of North America. We focused on the shapefile over CONUS – a two-dimensional smoke  
274 plume spatial depiction collapsing all plume stratifications to a satellite eye-view. For modeled plumes,  
275 we integrated modeled  $\Delta\text{CO}$  by multiplying the layer values with the corresponding CMAQ model layer



276 thicknesses and air density to derive a simulated smoke plume shape. HMS-derived smoke plume shape  
277 versus CMAQ predicted smoke plume shape was then used to evaluate the fire simulation.

278 Figure of Merits in Space (FMS) (Rolph et al., 2009) is a statistic for spatial analysis and was  
279 calculated as follows:

$$\text{FMS} = \frac{\text{Area}_{\text{hms}} \cap \text{Area}_{\text{cmaq}}}{\text{Area}_{\text{hms}} \cup \text{Area}_{\text{cmaq}}} \times 100\%$$

280 Where Area\_hms represents area of grid cells influenced by fire emission over CONUS detected by HMS  
281 and Area\_cmaq represents area of grid cells over CONUS identified by model prediction. In general, a  
282 higher FMS value indicates a better agreement between the observed and modeled plume shape (Rolph  
283 et al., 2009).

284 Figure 5 summarizes FMS during the SENEX campaign. Average FMS was 22% with its maximum  
285 at 56% on July 6 and minimum at 1.2% on June 17 2013. Figure 6a exhibits HMS detected smoke plume  
286 and CMAQ calculated smoke plume over CONUS on July 6. The light blue shading represents modeled  
287 plume shape (defined as total column  $\Delta\text{CO}$ ) and the thin dash line and emboldened green lines encircle  
288 areas representing HMS-derived light and strong influenced plume shape, respectively (Fig. 6a). The FMS  
289 score was 56% meaning that the modeled plume shape was consistent with that of HMS. However,  
290 CMAQ might have underestimated the intensive fire influence areas along the border of California and  
291 Nevada. Subsequently, the model also under-predicted its associated influence in North Dakota, South  
292 Dakota, Minnesota, Iowa and Wisconsin.

293 Figure 6b exhibits the worst case on June 17 2013 in terms of resulting with a FMS score at 1.2%.  
294 Two reasons led to this: (i) CMAQ missed fire emissions from Canada. Those fire sources located outside  
295 the CONUS modeling domain and our simulation system used a climatologically-based static LBC;  
296 Secondly on June 17, there were a lot of fire hotspots in the Southeastern U.S., i.e., in Louisiana,



297 Arkansas and Mississippi along the Mississippi River. Hotspots were detected but they lacked associated  
298 smoke in corresponding RGB imagery (Fig. 6c). This could be due to cloud blockage or to small  
299 agricultural debris clearing, burns in under-bushes or prescribed burns. These conditions prevented the  
300 HMS from identifying fires and hence emissions were not modeled for those sources.

301 It is noteworthy that the FMS evaluation contained uncertainties contributed from both  
302 modeled and observed values. The calculated campaign duration and SENEX-wide averaged FMS was  
303 22%. It is significantly higher than that achieved by a similar analyses done by HYSPLIT (Hybrid Single  
304 Particle Lagrangian Integrated Trajectory) smoke forecasting for the fire season of 2007 (6.1% to 11.6%)  
305 (Rolph et al., 2009). The primary reason is that the HYSPLIT smoke simulation accessed at the invocation  
306 of a forecast cycle the HMS fire information which is already one day old due to retrieval latency and  
307 cycle-queuing issues. However, our model simulation in this study was from a retrospective module  
308 using current day HMS fire information. Such discrepancies have been discussed by Huang et al. 2018  
309 (*manuscript in preparation*). Other reasons, such as plume rise, etc. were discussed in the following  
310 section on ASDTA.

### 311 **ASDTA**

312 The Automated Smoke Detection and Tracking Algorithm (ASDTA) is a combination of two data  
313 sets: (1) the NOAA Geostationary satellite (G13) retrieves aerosol optical depth using visible channels  
314 and produces a product called GOES Aerosol/Smoke Product (GASP) (Prados et al., 2007); and, (2) the  
315 NOAA HYSPLIT dispersion model predicts smoke plume direction and extension (Draxler and Hess 1998).  
316 ASDTA provides the capability to determine whether the GASP is influenced by one or multiple smoke  
317 plumes over a location at a certain time. The ASDTA is a signature identification analysis. On the other  
318 hand, the HYSPLIT smoke forecast is based on the HMS fire detection and BlueSky emission modeling  
319 driven by the NOAA NWS regional meteorology model. These data are suitable for model performance



320 evaluation in this study. For each simulation, modeled AOD was calculated for each sensitivity test  
321 (“with-fire” or “without-fire”) and  $\Delta$ AOD is defined as the difference obtained by subtracting  
322 AOD<sub>without-fire</sub> from AOD<sub>with-fire</sub>.

323 Figure 7a illustrates a GOES retrieved AOD (summed over from 10:00 am to 2:00 pm at local  
324 time) contour plot that reflects influences by smoke plumes over the CONUS domain on June 14 2013.  
325 Color-shaded region represents the fire-smoke influenced areas and the color denotes the magnitude of  
326 the retrieved AOD (Fig. 7a). Figure 7b presents similar results, but for simulated  $\Delta$ AOD (with-fire –  
327 without-fire). For further evaluation of the HMS detected smoke plume shape Fig. 7c can be compared  
328 with Figs. 7a and 7b.

329 Figure 7a shows several regions under the influence of fires in: California, northwest Mexico,  
330 Kansas, Missouri, Oklahoma, Arkansas, Texas and part of the Gulf of Mexico. In the northeastern USA,  
331 fire plumes occurred sparingly. Those regions agreed relatively well with the shaded contours between  
332 Figs. 7a and 7c. However, due to the lack of fire treatments in the CMAQ LBC, the simulation (Fig. 7b)  
333 missed smoke influence on the northeast region of the CONUS domain. CMAQ also failed to simulate  
334 the fire influences in the southwest region of the domain.

335 Similar plots for June 25 are shown in Figs. 7d, 7e and 7f for ASDTA, CMAQ and HMS,  
336 respectively. The ASDTA (Fig. 7d) predicted an overestimation in fire influences in the south including  
337 Texas and the Gulf of Mexico and an underestimation in the northeastern U.S. On the other hand, the  
338 model predicted two strong fire signals clearly: near the border between Arizona and Mexico, and in  
339 Colorado (See Fig. 7e). All the fire influenced areas in Fig. 7e were seen in Fig. 7f --- reflecting  
340 observation by HMS.

341 Comparing ASDTA plots and CMAQ  $\Delta$ AOD plots (Fig. 7a vs 7b; Fig. 7d vs 7e), we found both  
342 similarities and differences. Similarities were attributable to similar fire accounting, smoke emissions



343 from fires calculation and meteorology. Differences were attributable to: (i) HYSPLIT smoke simulation  
344 used more fire hotspots than that used by CMAQ due to domain size; (ii) only fires inside the CONUS  
345 were included in the CMAQ fire simulation and LBCs did not vary to reproduce impacts of wildfires from  
346 outside of the domain; (iii) Despite both the HYSPLIT and CMAQ fire plume rise were estimated by the  
347 Briggs' equation, the HYSPLIT plume rise was limited to 75% of the mixed layer height (MLH) at daytime  
348 and two times MLH at nighttime, whereas the CMAQ fire plume rise did not have these limitations.

#### 349 **SENEX**

350 SENEX (Southeast Nexus) was a field campaign conducted by NOAA in cooperation with the US  
351 EPA and the National Science Foundation in June and July 2013. Although SENEX was not specifically  
352 designed for fire studies, its airborne measurements included PM<sub>2.5</sub> OC and EC, CO and acetonitrile  
353 (CH<sub>3</sub>CN). CH<sub>3</sub>CN was chosen as a fire tracer since it is predominantly emitted from biomass burning  
354 (Holzinger et al., 1999; Singh et al., 2012).

355 CH<sub>3</sub>CN has a residence time in the atmosphere of around 6 months (Hamm and Warneck 1990)  
356 and the reported CH<sub>3</sub>CN background concentration is around 100 - 200 ppt (Singh et al., 2003).  
357 Measured CH<sub>3</sub>CN concentrations tend to increase with altitude (Singh et al., 2003; de Gouw et al., 2003),  
358 since biomass burning plumes are subject to ascend during long-range transport. During SENEX,  
359 measured CH<sub>3</sub>CN showed a similar pattern. Fire signals were identified through airborne measurements  
360 of CH<sub>3</sub>CN when its concentration exceeded the background; e.g., on July 3 2013, or when its  
361 concentration peak appeared at high altitude; e.g., on June 16 2013 and July 10 2013.

362 CH<sub>3</sub>CN airborne measurements were used to identify fire plumes at certain locations and  
363 heights during SENEX. For model evaluations, fire locations and accurate meteorological wind field are  
364 crucial to interpret 2-D measurements such as IMPROVE, HMS and ASDTA. To verify a 3-D fire field, it is  
365 critical to capture plume rise. However, it was extremely difficult to back out plume rise from the



366 airborne measurements. An additional uncertainty arose in the difference of temporal resolutions of the  
367 data: IMPROVE, HMS shapefiles and ASDTA were daily or hourly data, whereas airborne CH<sub>3</sub>CN data  
368 were measured at one-minute intervals.

369 Figure 8a shows a CMAQ simulated  $\Delta$ CO vertical distribution along flight transects on June 16  
370 2013. The x-axis label is UTC (hour) and the y-axis label is AGL (m). Two color bars represent observed  
371 CH<sub>3</sub>CN concentration (rectangle bar in ppt) and simulated  $\Delta$ CO concentration (fan bar in ppb),  
372 respectively. This flight occurred during the weekend over and around power plants around Atlanta, GA.  
373 The color of flight path represents observed CH<sub>3</sub>CN concentration in ppt. In Fig. 8a, the concentration of  
374  $\Delta$ CO increased from surface to 5000 m, especially above 2000 m. Six CH<sub>3</sub>CN concentration peaks were  
375 observed when AGL was above 2500 m.

376 For CMAQ simulated  $\Delta$ CO, five out of six fire signals detected by CH<sub>3</sub>CN measured spikes were  
377 captured where  $\Delta$ CO concentrations were all above 3 ppb. Only one fire signal was missed by the model  
378 at 18:30 UTC June 16 2013. Model simulation showed that long range transports (LRT) of smoke plumes  
379 influenced airborne observations. Fire signals from the free troposphere subsided and influenced flight  
380 measurements. High EC or OC or CO did not concur with high CH<sub>3</sub>CN observation probably due to  
381 species lifetime differences. HMS smoke plume did not show any hotspots or smoke plume around  
382 Atlanta suggesting that the sources of those observed fire signals were not from its vicinity.

383 A similar phenomenon was seen in SENEX flight 0710, which occurred during flight transects  
384 from Tennessee to Tampa, FL. Figure 8b is a similar graph as Fig. 8a. Based on  $\Delta$ CO concentrations,  
385 CMAQ captured the July 10 case as fire signals were observed. Nonetheless,  $\Delta$ CO may be over predicted  
386 at around 19 UTC. The model exhibited a fire signal with  $\Delta$ CO concentration of about 3 ppb near 6000 m  
387 around 19 UTC, whereas measured CH<sub>3</sub>CN was 120 ppt and decreased with AGL.



### 388 **SENEX flight on July 3**

389 Observations from IMPROVE, HMS and SENEX identified fire signals on July 3 2013. ASDTA  
390 retrievals were not available. Those signals were missed by the model. In this section, we will use all of  
391 evaluation methods addressed above to study potential causes of failure of the model to reproduce fire  
392 signals.

393 At the MACA IMPROVE site on July 3 2013, the wind direction at the surface was southeasterly,  
394 with no fire hotspots (solid black circle) located upwind of MACA (Fig. 9a). Without any identified  
395 hotspots upwind, the model missed fire signals observed at MACA on July 3 2013.

396 Flight #0703 was a night mission targeting power plants in Missouri and Arkansas. The flight  
397 path is shown in Fig. 9b and is colored by measured CH<sub>3</sub>CN concentration. In order to highlight CH<sub>3</sub>CN  
398 concentrations above 400 ppt in the measurements, CH<sub>3</sub>CN concentrations below 400 ppt was  
399 represented by black dots. During the flight, 16 measurements of acetonitrile concentration above 400  
400 ppt were observed and the maximum was 3227.9 ppt. These observations were located over  
401 northwestern Tennessee and close to the borders of Kentucky, Illinois, Missouri and Arkansas. Except  
402 for one observation, the flight ASL was between 500 m and 1000 m.

403 Enhancements of CO and OC were also measured concurrently with CH<sub>3</sub>CN. Figures 9c and 9d  
404 show scatter plots for CH<sub>3</sub>CN versus CO and OC, respectively. Measured CH<sub>3</sub>CN was highly correlated to  
405 both measured CO and OC, with linear correlation coefficients ( $R^2$ ) of 0.83 and 0.71, respectively. The  
406  $\Delta\text{CH}_3\text{CN}/\Delta\text{CO}$  ratio is around 2.7 (ppt/ppb) --- consistent with findings of other measurements over  
407 California in 2002 when a strong forest fire signal was intercepted by aircraft (de Gouw et al., 2003). The  
408  $\Delta\text{CH}_3\text{CN}/\Delta\text{CO}$  ratio was around 6.85 (ppt/(mg m<sup>-3</sup>)) ---- in the range of biomass burning analyses in  
409 MILAGRO (Megacity Initiative Local and Global Research Observations) (Aiken et al., 2010).



410 Figure 9e shows model simulated  $\Delta\text{CO}$  with peaks at AGL below 3000 m. Fire signals showed  
411 substantial influences on aircraft measurement at around 5 UTC. However, clear fire signals between 2  
412 UTC and 3 UTC were observed based on prior  $\text{CH}_3\text{CN}$  analysis. The model either predicted insufficient  
413 fire emission influences or missed it. FMS score on July 3 was 30%. Figure 9f shows that CMAQ did not  
414 predict plumes where the HMS plume analysis exhibited several dense smoke plumes. As NOAA Smoke  
415 Text Product (<http://www.ssd.noaa.gov/PS/FIRE/DATA/SMOKE>) described on its July 03 0501 UTC  
416 report: a smaller very dense patch of remnant smoke, analyzed earlier the same day over southern  
417 Missouri, drifted southward into Arkansas.”

418 The reasons the model missed these fire observations were not clear. Figures 10, 11a and 11b  
419 suggest a few clues. Figure 10 is a backward trajectory analysis plot for the observations obtained during  
420 the SENEX flight on July 3 with  $\text{CH}_3\text{CN}$  measured concentration above 400 ppt. Both the transect and  
421 flight altitude of the air parcels clearly showed those measurements were most likely influenced by the  
422 nearby pollution sources. Figure 11a illustrates the locations of fire used in the CMAQ simulation. It is  
423 noted that hmsysplit.txt is input into BlueSky after HMS quality control (Fig. 1). There were several  
424 hotspots around the region where the IMPROVE site MACA was located and where the SENEX flight  
425 overpassed. Our fire simulation system might have underestimated smoke emissions from those fires.  
426 Other explanation was from Fig. 11b, which illustrated hotspots in hmx.txt. In hmx.txt --- showing every  
427 detected fire spots by HMS before quality control. Comparing Fig. 11a with 11b, there were clusters of  
428 fire spots in the central U. S. especially in West Tennessee. However, those spots were removed during  
429 the HMS quality control process because there were no associated smoke plumes visible. In most of  
430 times, those fires were believed to be small sized fires such as from agriculture fires or prescribed burns.  
431 For this case, there seem to have been thin clouds overhead and thicker clouds in the vicinity,  
432 (<http://inventory.ssec.wisc.edu/inventory/image.php?sat=GOES-13&date=2013-07->



433 03&time=16:02&type=Imager&band=1&thefilename=goes13.2013.184.160147.INDX&coverage=CONUS  
434 &count=1&offsetz=0), so it would be hard to differentiate smoke from clouds by satellite observations

## 435 **CONCLUSIONS**

436 In support of the NOAA SENEX field experiment in June-July 2013, simulations were conducted  
437 including smoke emissions from fires. In this study, a system accounting for fire emissions in a chemical  
438 transport model is described, including a satellite fire detecting system (HMS), a fire emission calculation  
439 model (BlueSky), a pre-processing of fire emissions (SMOKE), and simulation over the SENEX domain by  
440 CMAQ. The focus of this work is to evaluate the system's capability to capture fire signals identified by  
441 multiple observation data sets. These data sets included IMPROVE ground station observations, satellite  
442 observations (HMS plume shapefile and ASDTA) and airborne measurements from the SENEX campaign.

443 For IMPROVE data, potential fire signals were identified by measured potassium concentrations  
444 in  $PM_{2.5}$ . Fire identifications in CMAQ rely on its predicted  $\Delta CO$  and the difference between simulations  
445 with and without fire emissions. Three out of four observed fire signals were captured by CMAQ  
446 simulations. For HMS smoke plume shapefiles that were manually plotted by analysts to represent the  
447 regions impacted by smoke, we used FMS to calculate the percentage of its overlapping with CMAQ  
448 predicted smoke plumes. FMS averaged 22% over forty days of the SENEX campaign. In terms of fire  
449 smoke impacts on  $\Delta AOD$ , both ASDTA and CMAQ showed similar patterns that were compared with  
450 HMS plume shapefile analysis. In terms of measured  $CH_3CN$ , a biomass burning plume tracer, both  
451 SENEX aircraft in-flight measurements and CMAQ simulations captured signatures of long range  
452 transport of fire emissions.

453 Generally, using HMS-detected fire hotspots and smoke data was useful for predictions of fire  
454 impacts and their evaluation. The HMS-BlueSky-SMOKE-CMAQ fire simulation system, which is also used



455 in NAQFC, was able to capture most of the fire signals detected by multiple observations. However, the  
456 system failed to identify fire cases on June 17 and July 3 2013 -- thereby demonstrating two problems  
457 with the simulation system. One identified problem was the lack of a dynamical fire LBC outside the  
458 CONUS domain to represent the inflows of strong fire signals originating from outside the simulation  
459 domain. Secondly, the HMS quality control procedure eliminated fire hotspots that were not associated  
460 with visible smoke plumes leading to an underestimation.

461 We were keen on understanding and quantifying the various uncertainties and observational  
462 constraints of this study therefore the following rules of thumb were observed: (1) A holistic evaluation  
463 approach was adopted so that the fire smoke algorithm was interpreted as a single entity to avoid  
464 impasse arose by uncertainties specific to the different components in the system, (2) Analysis  
465 conclusion applicable to the entire simulation period was drawn so that the episodic characteristics of  
466 the cases embedded in the simulation were averaged and generalized. This new methodology may  
467 benefit NAQFC, (3) We took advantage of the multiple perspectives of the observation systems that  
468 offered a wide spectrum of temporal and spatial variabilities intrinsic to the systems, and (4) We were  
469 intentional to be conservative in discarding data so that we maximized the sampling pool for statistical  
470 analysis and avoided unwittingly discarding poorly simulated cases, good out-layers, and weak sparse  
471 but accurate signals.

472 Quantitative evaluation of fire emissions and their subsequent influences on ozone and  
473 particulate matter in this fire and smoke prediction system is challenging. Future work includes applying  
474 these findings to the NAQFC and improving the NAQFC system's capabilities to simulate fires accurately.



## 475 **Code Availability**

476 The source code used in this study is available online at

477 <http://www.nco.ncep.noaa.gov/pmb/codes/nwprod/cmaq.v5.0.2>.

## 478 **Acknowledgements & disclaimer**

479 This work was partially funded by the NASA Air Quality Applied Sciences Team (AQAST), project  
480 grant NNH14AX881. The authors are thankful to Dr. Joost De Gouw and Dr. Martin G. Graus of the Earth  
481 System Research Laboratory, NOAA for sharing the SENEX campaign data used in this study. Although  
482 this work has been reviewed by the Air Resources Laboratory, NOAA and approved for publication it  
483 does not necessarily reflect their policies or views.

## 484 **Figures:**

485 Figure 1, Fire emission calculation and smoke plume simulation algorithm.

486 Figure 2, in 4km SENEX domain, (a): the contribution (%) of CO emission from fires occurred inside the  
487 SENEX domain; (b): the contribution (%) of CO flux flowing into the SENEX domain from its boundary  
488 caused by fires burning outside the SENEX domain but inside the CONUS domain.

489 Figure 3, simulated  $\Delta\text{CO}$  (ppb) extracted along SENEX flight path.

490 Figure 4,  $\Delta\text{CO}$  (>2.0 ppb) simulated in SENEX domain on June 24 2013. The solid circle is detected fire  
491 hotspots by HMS. The open triangle represents IMPROVE sites.

492 Figure 5, FMS (Figure of Merits in Space) (%) from June 11 to July 19 in 2013 during SENXE experiment.

493 Figure 6, HMS observed plume shape versus CMAQ predicted plume shape on (a): July 6 2013; (b): June  
494 17 2013; The light blue shading represents modeled plume shape (defined as total column  $\Delta\text{CO}$ ) and the  
495 thin dash line and emboldened green lines encircle areas representing HMS-derived light and strong  
496 influenced plume shape, respectively. (c): HMS observed fire hotspots (red) and plume shapes (white)  
497 (<http://ready.arl.noaa.gov/data/archives/fires/national/arcweb>) on June 17, 2013.

498 Figures 7, GOES detected AOD influenced by fires using ASDTA diagnose method. Color-shaded region  
499 represents the fire-smoke influenced areas and the color denotes the magnitude of the retrieved AOD  
500 on (a): June 14 2013; (d): June 25 2013;  $\Delta\text{AOD}$  (with-fire – without-fire) simulated in CMAQ on (b): June



501 14 2013; (e): June 25 2013; HMS observed fire hotspots (red) and plume shapes (white)  
502 (<http://ready.arl.noaa.gov/data/archives/fires/national/arcweb>) on (c ): June 14 2013; (f): June 25 2013.

503 Figure 8, CMAQ simulated  $\Delta\text{CO}$  vertical distributions along SENEX flight transect on (a): June 16 2013;  
504 (b): July 10 2013; The x-axis label is UTC (hour) and the y-axis label is AGL (m). Two color bars represent  
505 observed  $\text{CH}_3\text{CN}$  concentration (rectangle bar in ppt) and simulated  $\Delta\text{CO}$  concentration (fan bar in ppb),  
506 respectively.

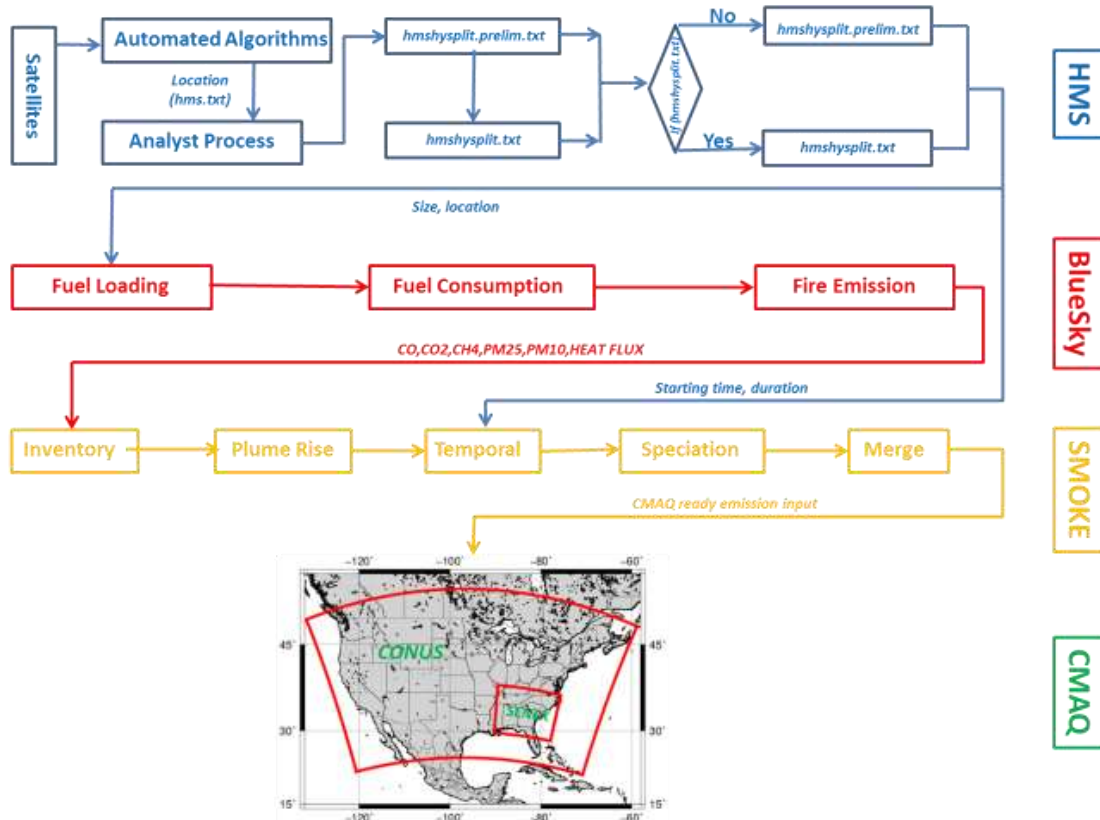
507 Figure 9, plots for July 3 2013 case, (a): IMPROVE; (b): the flight path of SENEX #0703 colored by  
508 measured  $\text{CH}_3\text{CN}$  concentration (ppt); (c):  $\text{CH}_3\text{CN}$  (ppt) vs CO (ppb); (d):  $\text{CH}_3\text{CN}$  (ppt) vs  $\text{AMS\_Org}$  ( $\text{mg m}^{-3}$ );  
509 (e): CMAQ simulated  $\Delta\text{CO}$  vertical distributions along flight transect; (f): HMS observed plume shape  
510 versus CMAQ prediction.

511 Figure 10, a backward trajectory analysis for the observations obtained during the SENEX flight on July  
512 03 2013 with  $\text{CH}_3\text{CN}$  measured concentration above 400 ppt.

513 Figure 11, detected fire hotspots on July 03 2013 (a): hmxhysplit.txt; (b): hmx.txt.

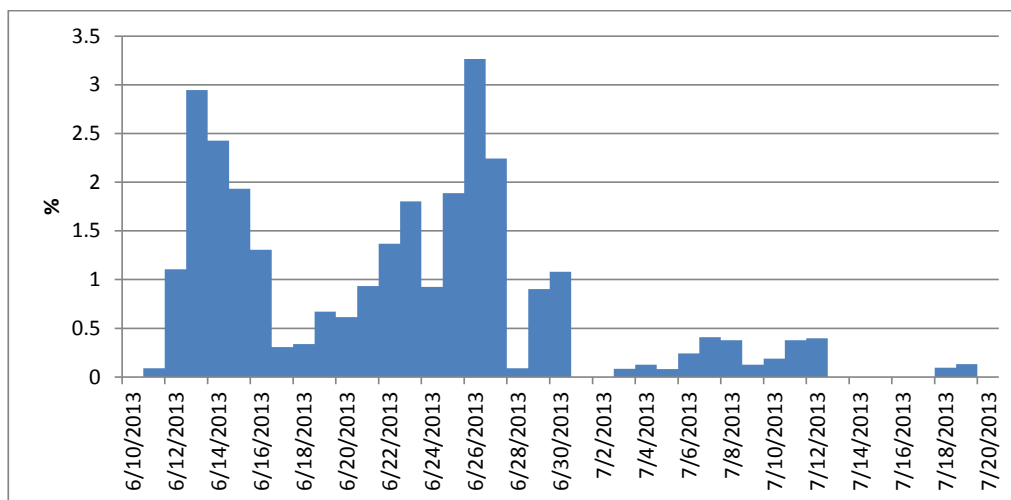
514

515



516  
 517  
 518  
 519

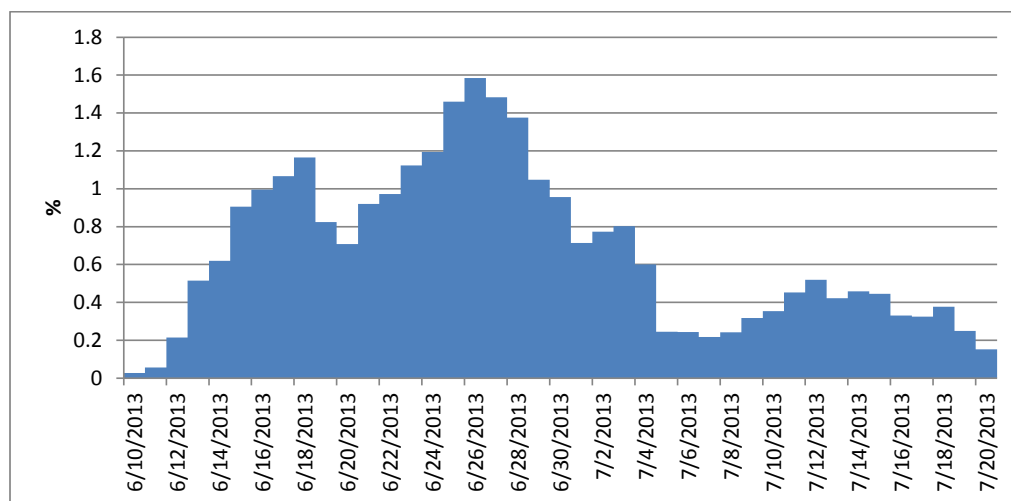
Figure 1: Fire emission calculation and smoke plume simulation algorithm



520

521

**Figure 2a: the contribution (%) of CO emission from fires occurred inside the SENEX domain**



522

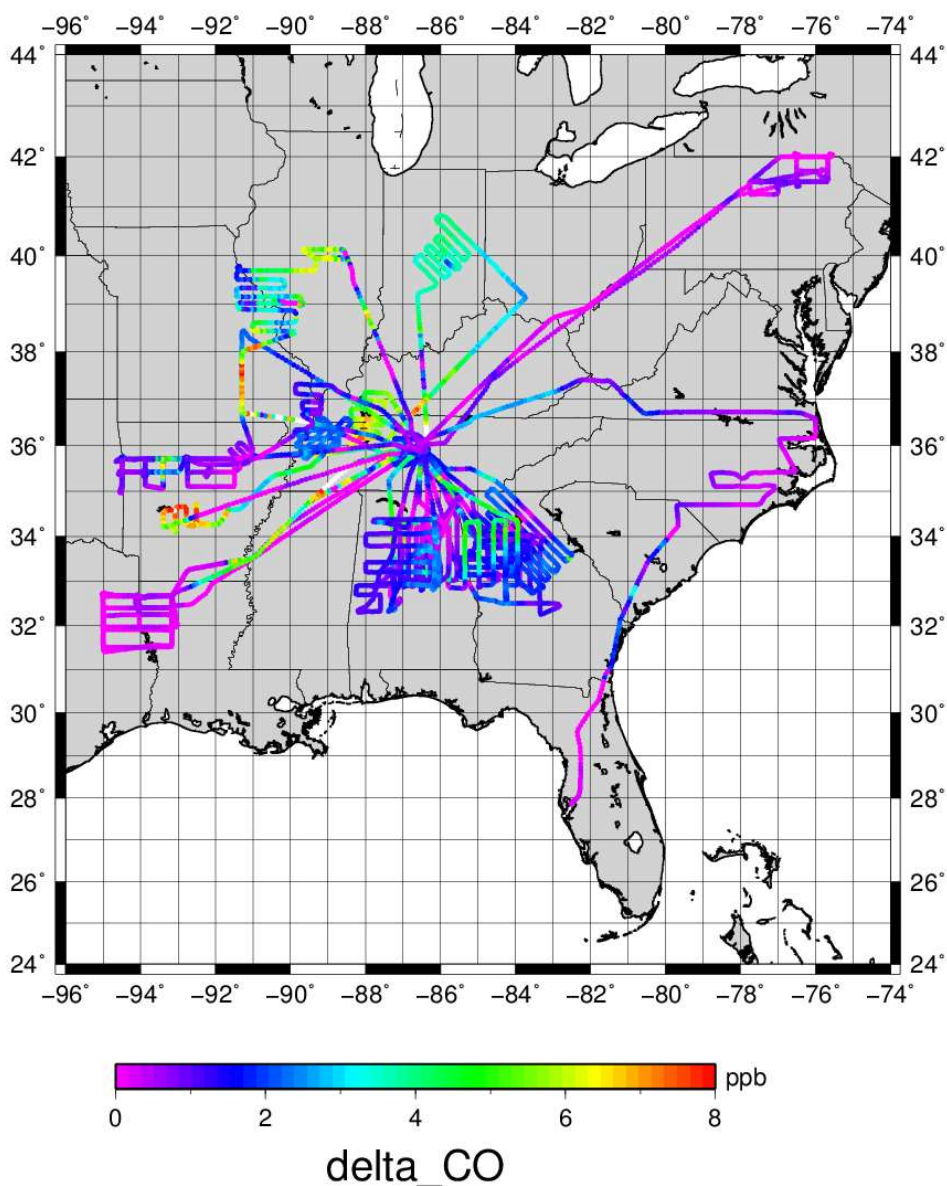
523

524

525

526

**Figure 2b: the contribution (%) of CO flux flowing into the SENEX domain from its boundary caused by fires burning outside the SENEX domain but inside the CONUS domain**

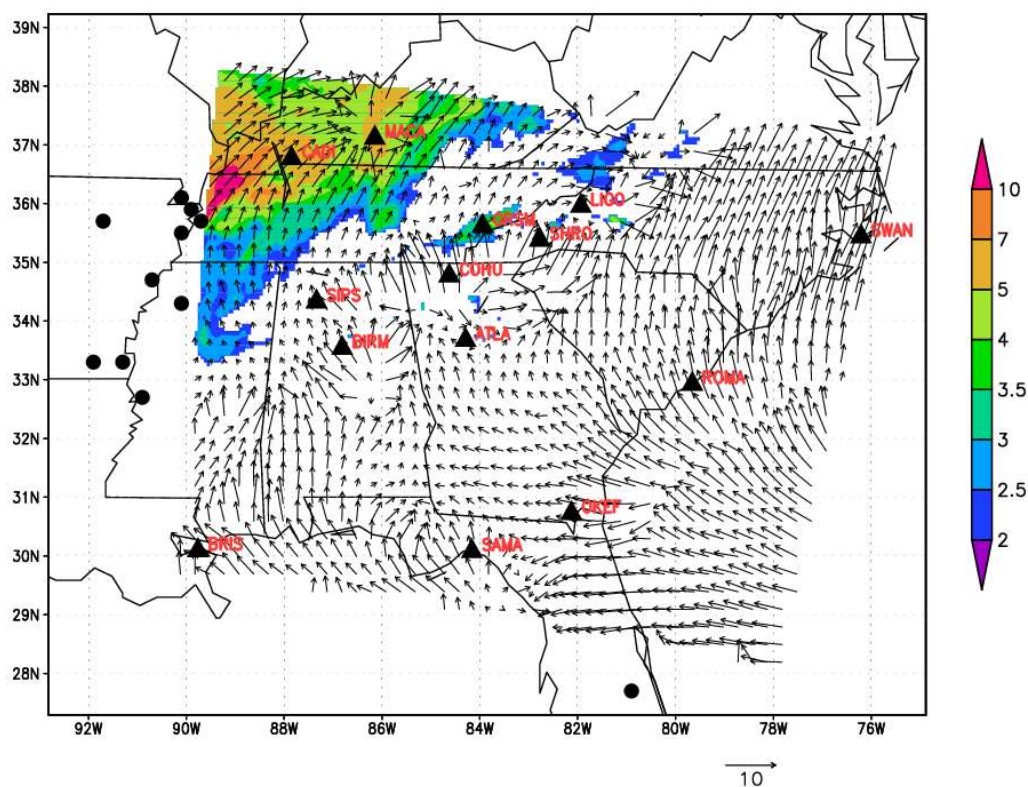


527

528

529

Figure 3: simulated  $\Delta\text{CO}$  (ppb) extracted along SENEX flight path



530

531 **Figure 4:  $\Delta\text{CO}$  (>2.0 ppb) simulated in SENEX domain on June 24 2013. The solid circle is detected fire**  
532 **hotspots by HMS. The solid triangle represents IMPROVE sites.**

533

534

535

536

537

538

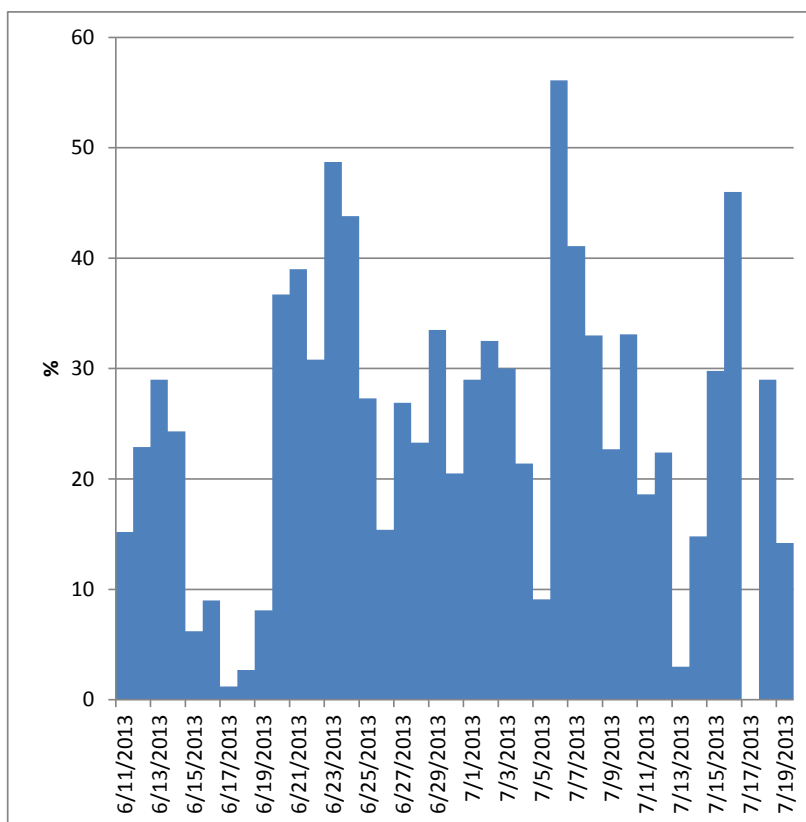
539

540

541



542



543

544 **Figure 5: FMS (Figure of Merits in Space) (%) from June 11 to July 19 in 2013 during SENXE experiment**

545

546

547

548

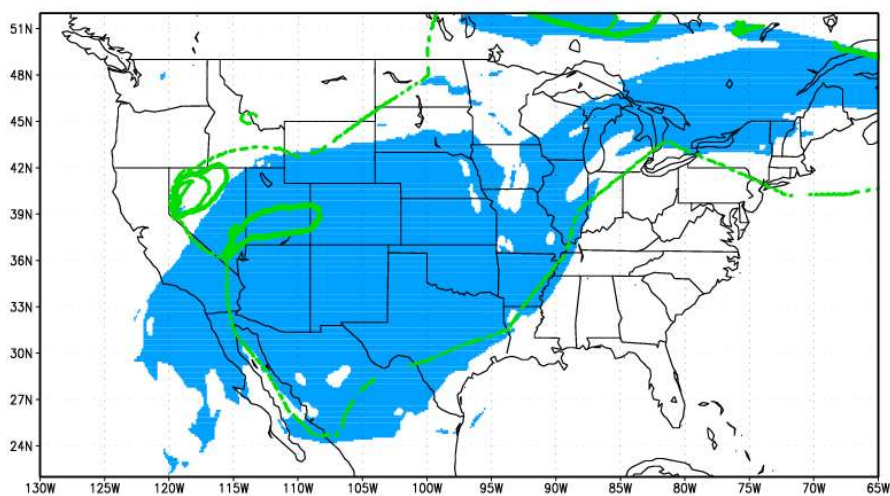
549

550

551

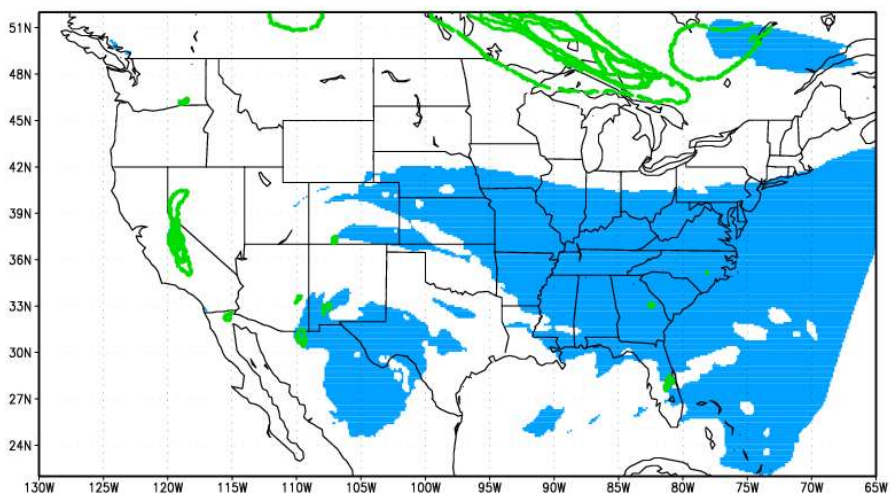
552

553



554

555 **Figure 6a: HMS observed plume shape versus CMAQ predicted plume shape on July 6 2013; The light**  
556 **blue shading represents modeled plume shape (defined as total column  $\Delta\text{CO}$ ) and the thin dash line**  
557 **and emboldened green lines encircle areas representing HMS-derived light and strong influenced**  
558 **plume shape, respectively.**

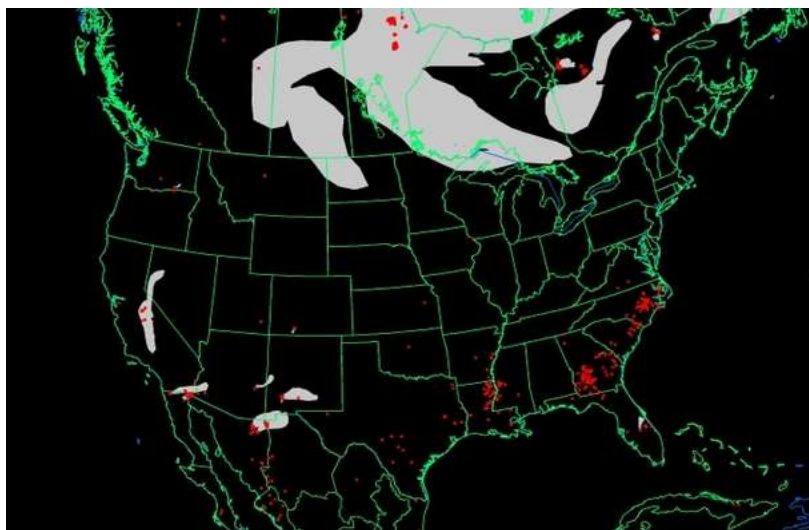


559

560

**Figure 6b: on June 17 2013**

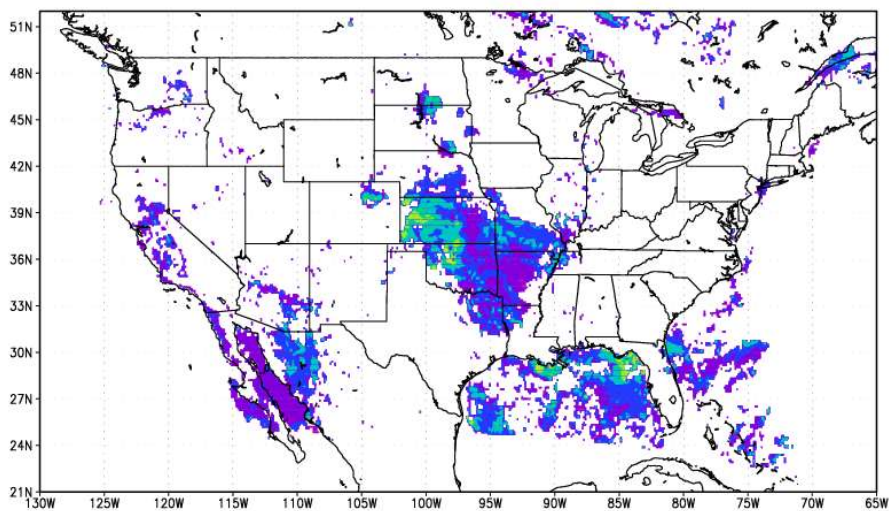
561



562

563 **Figure 6c: HMS detected fire hotspots (red) and smoke plume shapes (white) on June 17 2013**  
564 **(<http://ready.arl.noaa.gov/data/archives/fires/national/arcweb>)**

565

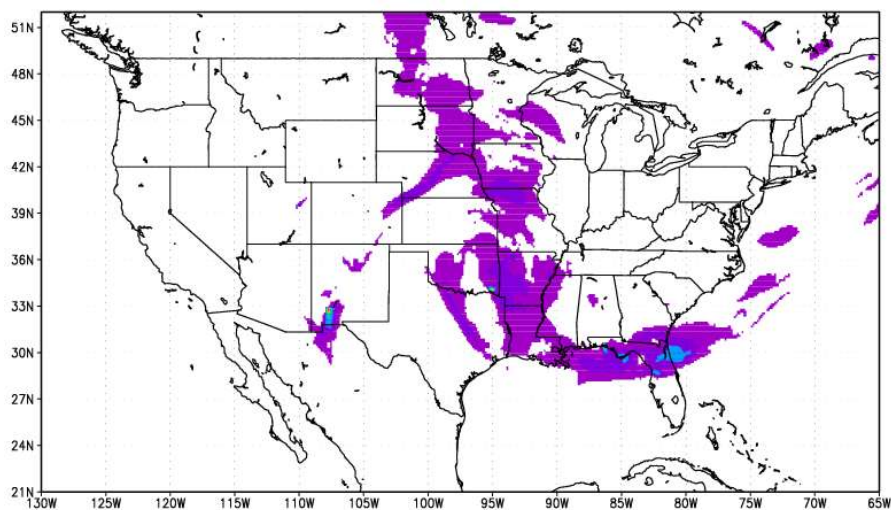


566

567 **Figure 7a: GOES detected AOD influenced by fires using ASDTA diagnose method on June 14 2013.**  
568 **Color-shaded region represents the fire-smoke influenced areas and the color denotes the magnitude**  
569 **of the retrieved AOD.**



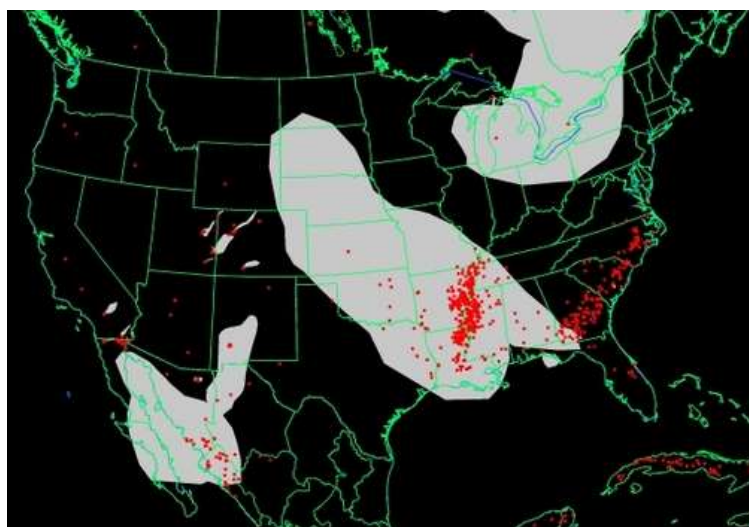
570



571

572

**Figure 7b: simulated  $\Delta$ AOD (with-fire – without-fire) in CMAQ on June 14 2013**



573

574

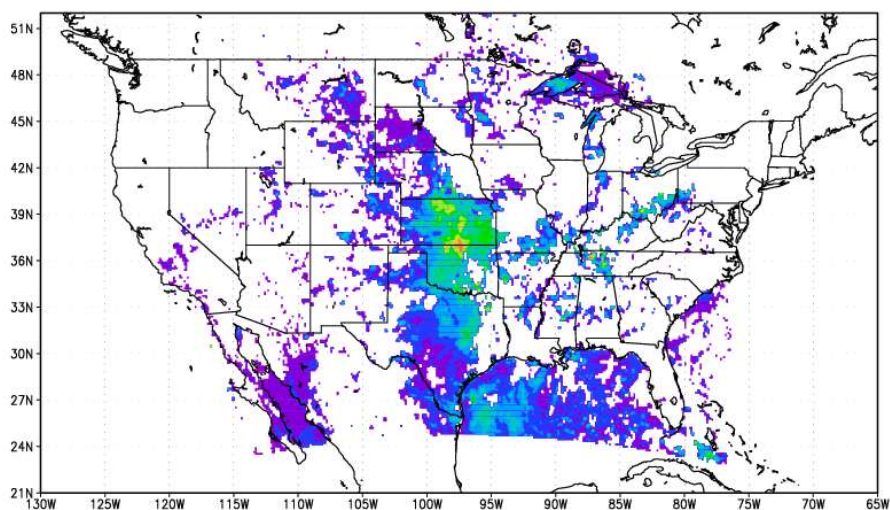
575

**Figure 7c: HMS detected fire hot spots (red) and smoke plume shapes (white) on June 14 2013**  
(<http://ready.arl.noaa.gov/data/archives/fires/national/arcweb>)

576

577

578

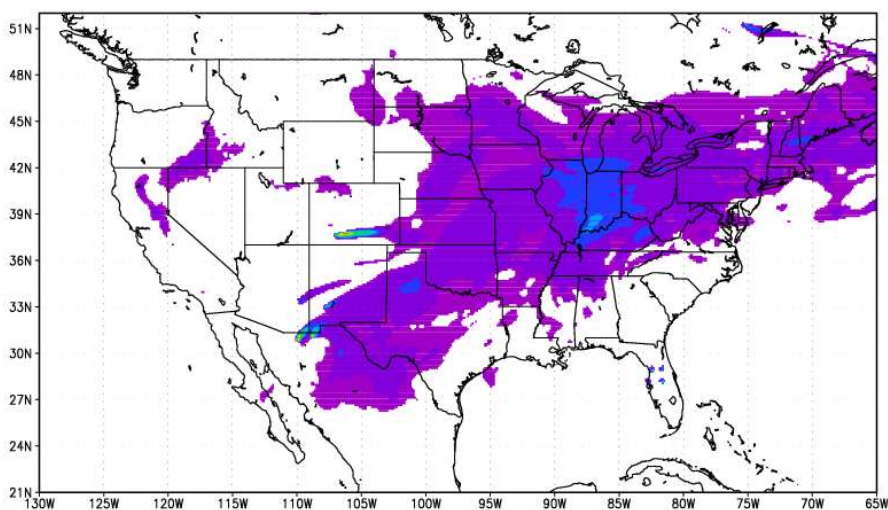


579

580 **Figure 7d: GOES detected AOD influenced by fires using ASDTA diagnose method on June 25 2013.**

581 **Color-shaded region represents the fire-smoke influenced areas and the color denotes the magnitude**

582 **of the retrieved AOD.**

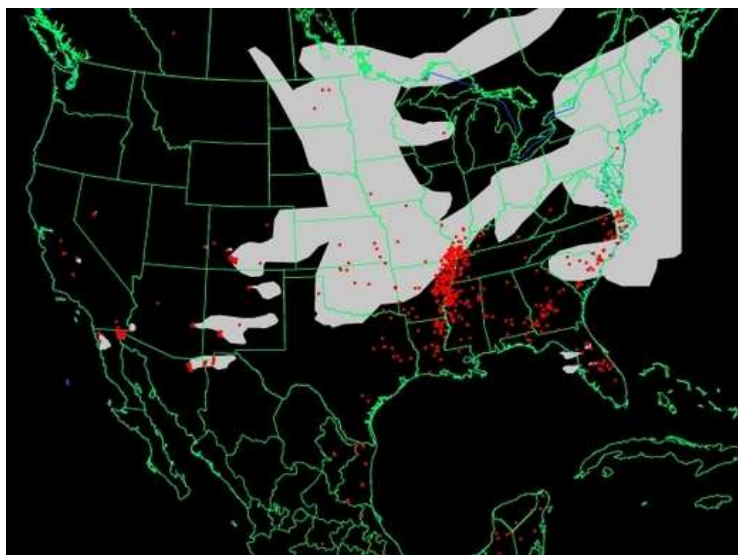


583

584 **Figure 7e: simulated  $\Delta$ AOD (withfire – nofire) in CMAQ on June 25 2013**

585

586

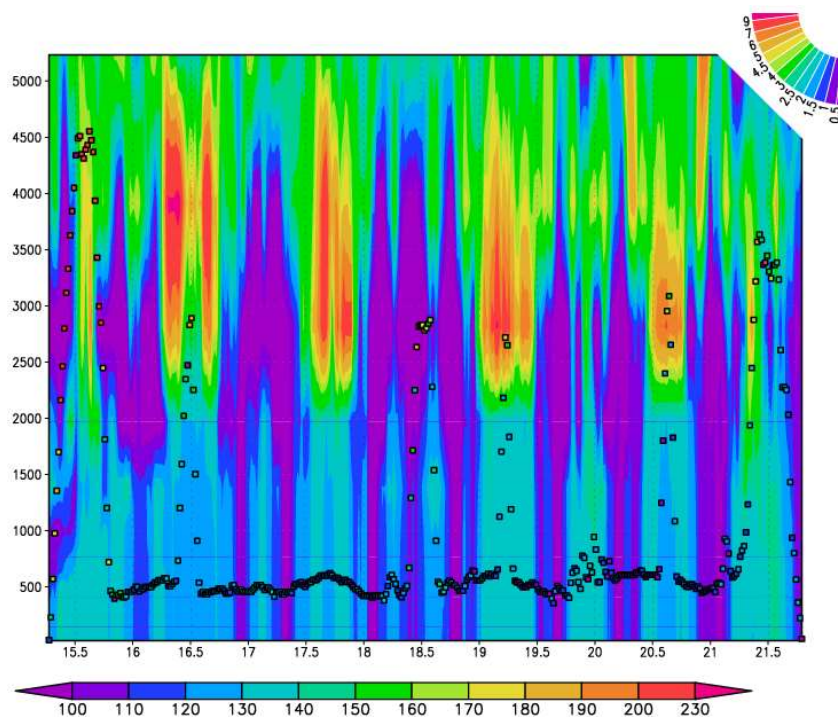


587

588 **Figure 7f: HMS detected fire hot spots (red) and smoke plume shapes (white) on June 25 2013**  
589 **<http://ready.arl.noaa.gov/data/archives/fires/national/arcweb>**

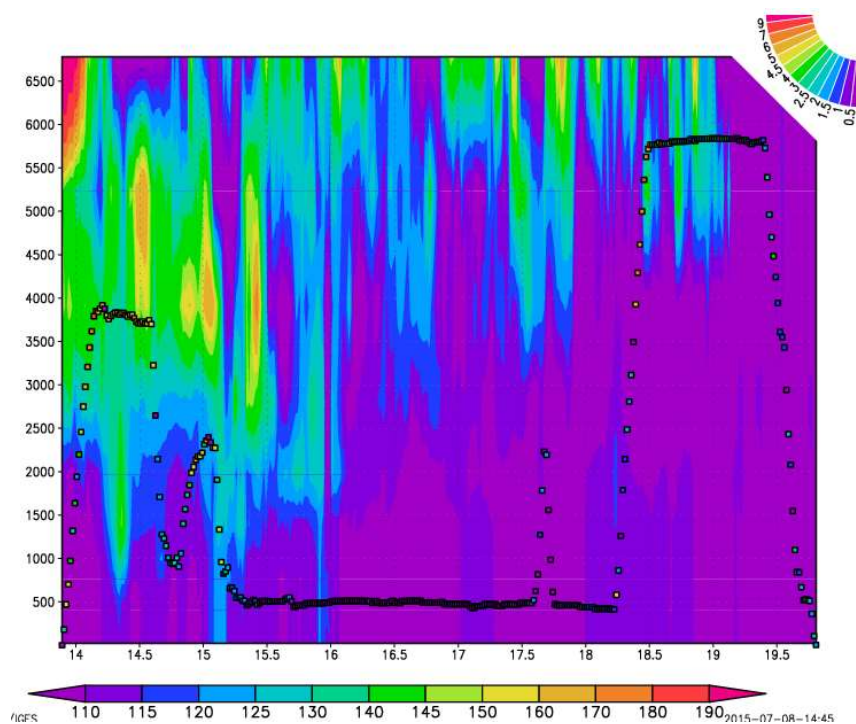
590

591



592

593 **Figure 8a: CMAQ simulated  $\Delta\text{CO}$  (ppb) vertical distributions along flight transect on June 16 2013. The**  
594 **x-axis label is UTC (hour) and y-axis label is AGL (m). Two color bars represent observed  $\text{CH}_3\text{CN}$**   
595 **concentration (rectangle bar in ppt) and simulated  $\Delta\text{CO}$  concentration (fan bar in ppb), respectively.**



596

597

598 **Figure 8b: CMAQ simulated  $\Delta\text{CO}$  (ppb) vertical distributions along flight transect on July 10 2013. The**  
599 **x-axis label is UTC (hour) and y-axis label is AGL (m). Two color bars represent observed  $\text{CH}_3\text{CN}$**   
600 **concentration (rectangle bar in ppt) and simulated  $\Delta\text{CO}$  concentration (fan bar in ppb), respectively.**

601

602

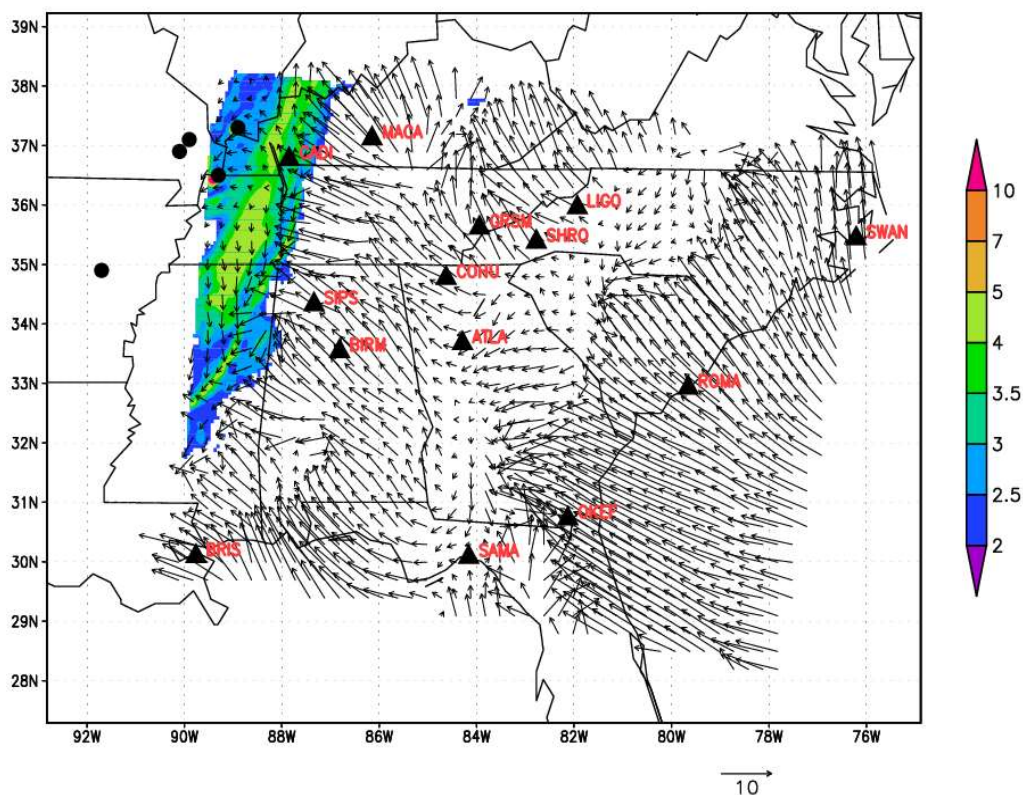
603

604

605

606

607



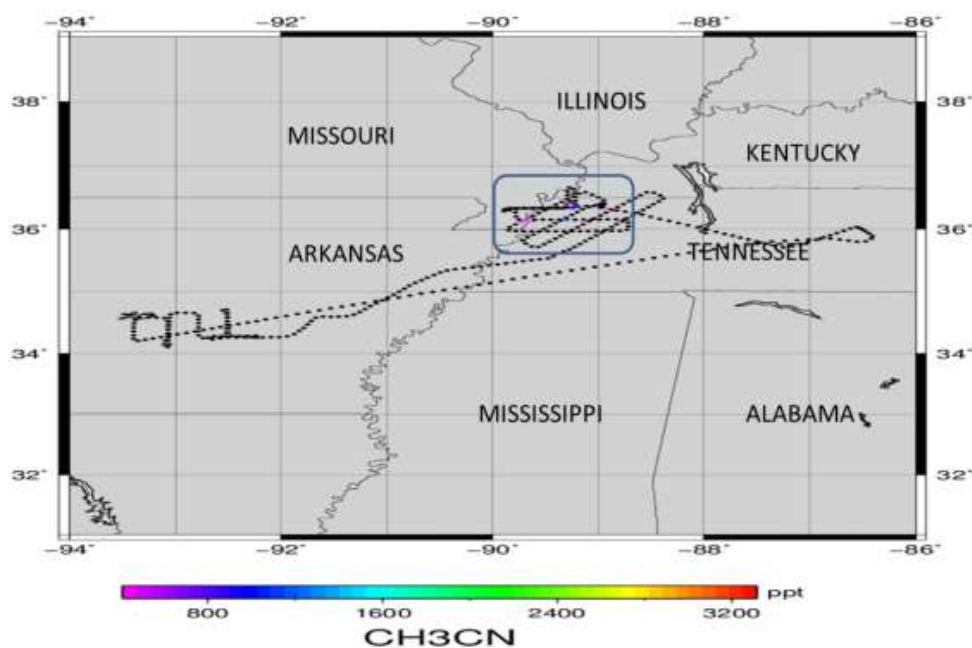
608

609 **Figure 9a:  $\Delta\text{CO}$  (>2.0 ppb) simulated in SENEX domain on July 03 2013. The solid circle is detected fire**  
610 **hotspots by HMS. The solid triangle represents IMPROVE sites.**

611

612

613



614

615 **Figure 9b: the flight path of SENEX #0703, colored by measured CH<sub>3</sub>CN concentration (ppt)**

616

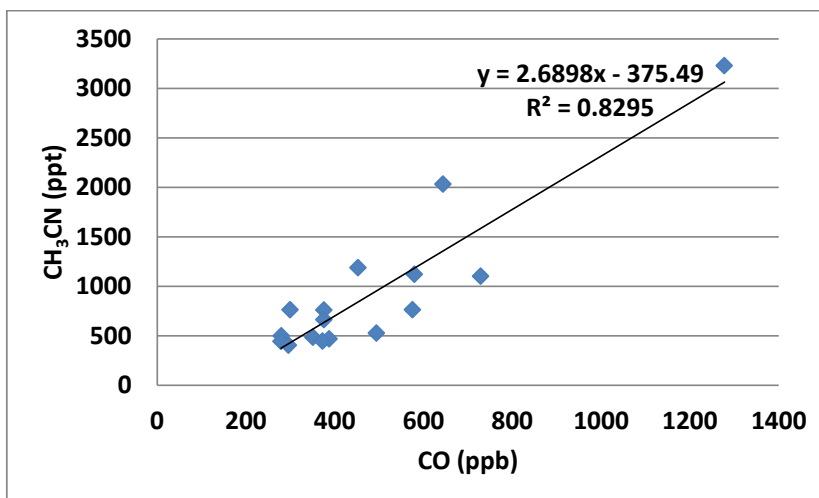
617

618

619

620

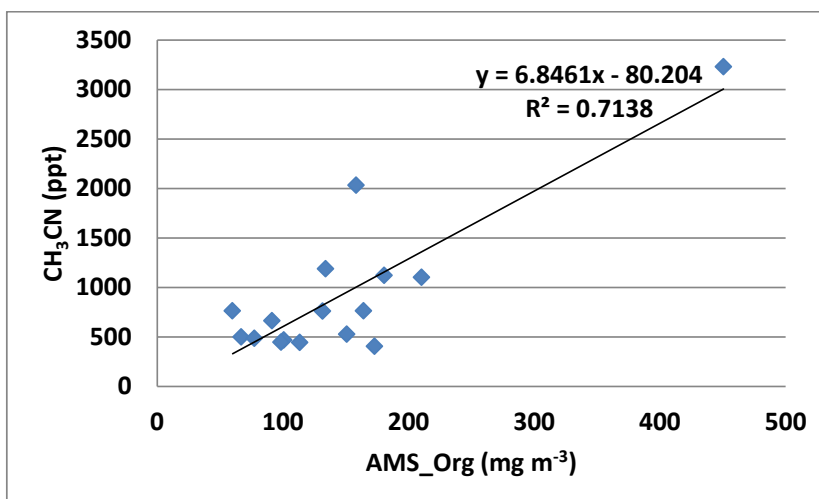
621



622

623

Figure 9c: CH<sub>3</sub>CN (ppt) vs CO (ppb)



624

625

626

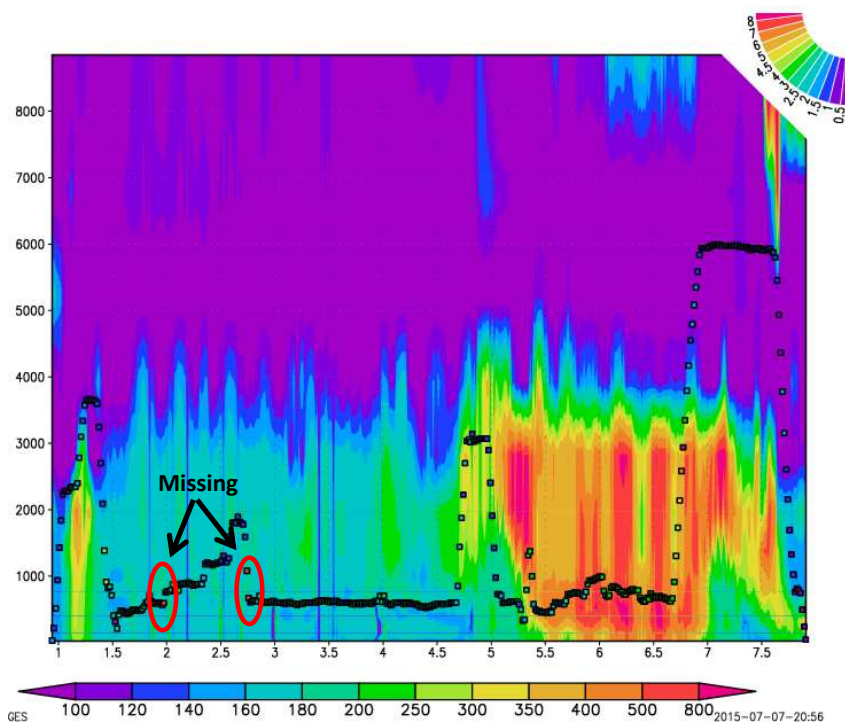
627

628

629

630

Figure 9d: CH<sub>3</sub>CN (ppt) vs AMS\_Org (mg m<sup>-3</sup>)

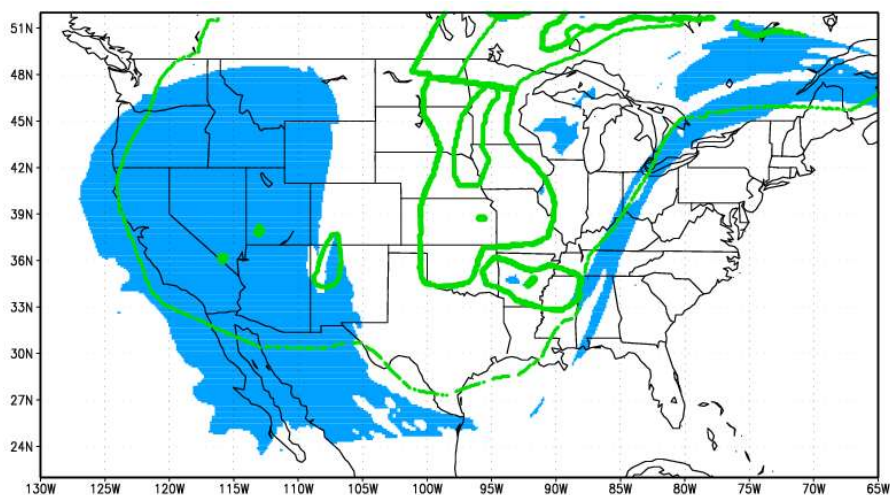


631

632 **Figure 9e: CMAQ simulated  $\Delta\text{CO}$  (ppb) vertical distributions along flight transect on July 03 2013. The**  
633 **x-axis label is UTC (hour) and y-axis label is AGL (m). Two color bars represent observed  $\text{CH}_3\text{CN}$**   
634 **concentration (rectangle bar in ppt) and simulated  $\Delta\text{CO}$  concentration (fan bar in ppb), respectively.**

635

636



637

638

639

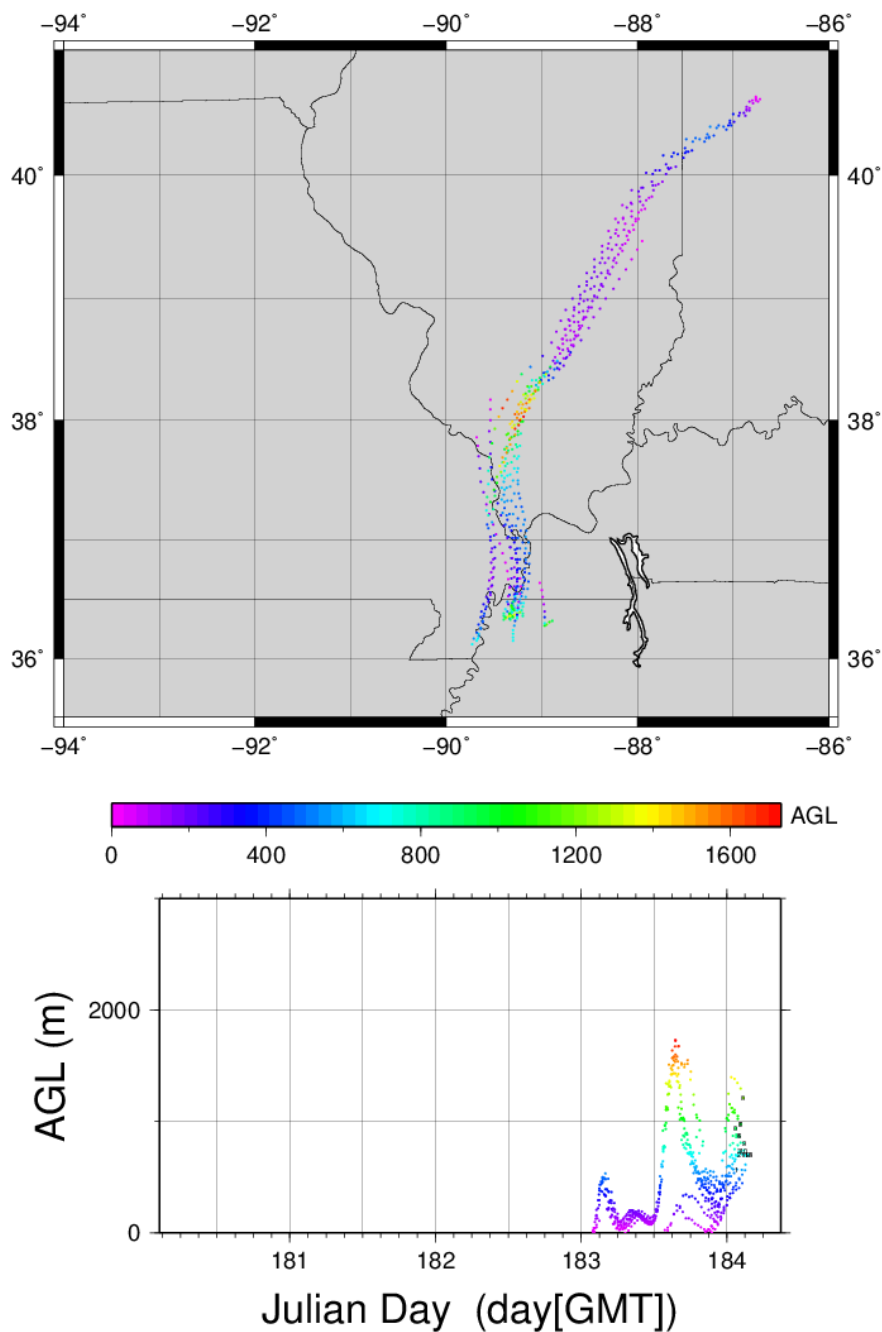
640

641

642

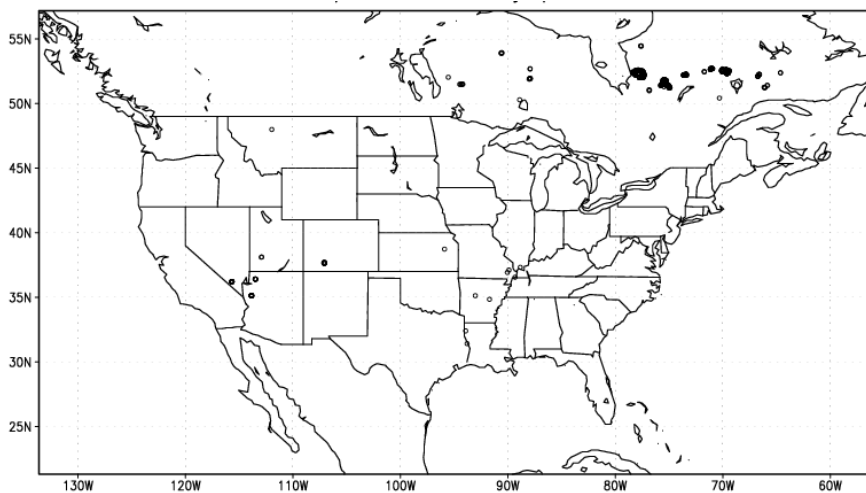
643

**Figure 9f: HMS plume shape versus CMAQ predictions on July 03 2013. The light blue shading represents modeled plume shape (defined as total column  $\Delta\text{CO}$ ) and the thin dash line and emboldened green lines encircle areas representing HMS-derived light and strong influenced plume shape, respectively.**



644

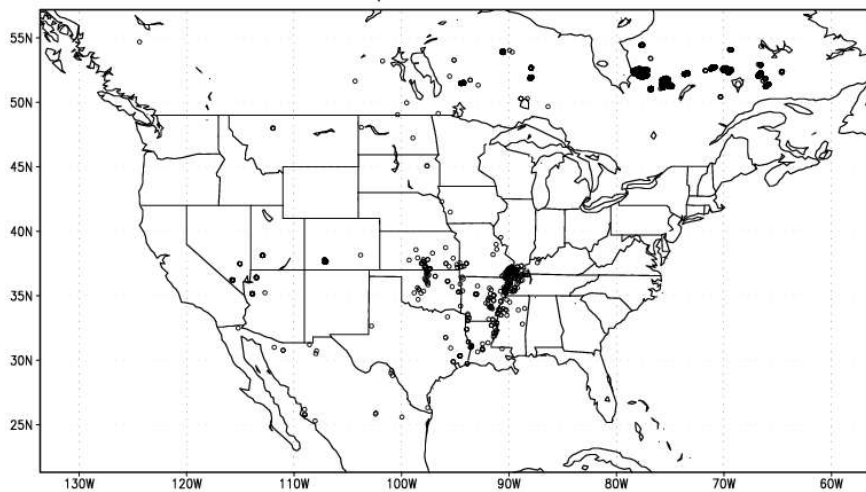
645 **Figure 10, a backward trajectory analysis for the observations obtained during the SENEX flight on July**  
646 **03 with CH<sub>3</sub>CN measured concentration above 400 ppt.**



647

648

**Figure 11a: fire hotspots in hmxhysplit.txt on July 03 2013**



649

650

651

652

653

654

655

**Figure 11b: fire hotspots in hmx.txt on July 03 2013**



656 **Tables:**

657 **Table 1: observed and simulated CO (ppb) during NOAA SENEX experiment**

AGL (m)	SAMPLE SIZE	OBS	OBS_MAX	Mod_withfire	Mod_nofire	ΔCO
<500	166	128.93±38.51	319.55	108.70±21.37	107.16±20.34	1.54
500~1000	3565	146.19±44.39	1277.97	108.39±19.82	106.50±18.86	1.88
1000~1500	793	125.41±28.09	299.64	100.11±15.63	98.49±14.67	1.62
1500~2000	306	119.68±23.99	265.29	100.75±17.04	99.08±15.89	1.67
2000~2500	219	111.48±19.98	286.22	99.88±17.95	98.37±16.92	1.51
2500~3000	209	111.84±19.79	295.79	97.43±12.21	95.87±11.15	1.56
3000~3500	181	109.31±16.66	197.94	89.34±12.09	88.13±11.06	1.21
3500~4000	195	110.78±14.36	140.42	92.11±10.73	90.25±9.62	1.86
4000~5000	369	89.82±19.09	138.04	80.36±10.15	79.17±9.14	1.19
5000~6000	354	102.26±22.37	209.20	78.12±7.64	76.82±6.28	1.30
6000~7000	85	87.53±17.88	115.32	73.35±4.71	70.58±2.45	2.77

658

659

660

661

662 **Table 2: identified fire signals from IMPROVE measurements during SENEX experiment**

Site	Date	Concentrations (ug m <sup>-3</sup> )						Concentration/Average						Ratio	
		EC	OC	K	SOIL	NO <sub>3</sub> <sup>-</sup>	SO <sub>4</sub> <sup>2-</sup>	EC	OC	K	SOIL	NO <sub>3</sub> <sup>-</sup>	SO <sub>4</sub> <sup>2-</sup>	BC/OC	K/BC
COHU	0621	0.28	2.10	0.05	0.22	0.13	2.61	1.4	1.46	1.42	0.39	0.84	1.28	0.1331	0.1933
MACA	0624	0.45	2.34	0.09	0.26	0.24	2.76	1.85	1.58	1.82	0.48	1.19	1.24	0.1929	0.1973
MACA	0703	0.33	2.32	0.08	0.16	0.29	2.11	1.35	1.57	1.73	0.29	1.43	0.94	0.1423	0.2554
BRIS	0703	0.24	0.98	0.21	0.31	0.11	2.63	1.49	1.28	2.79	0.13	0.35	1.36	0.2458	0.8851
GRSM	0621	0.25	1.56	0.05	0.24	0.13	2.52	1.36	1.45	1.24	0.49	0.99	1.42	0.1596	0.1979

663

664

665

666

667

668

669

670

671 **References:**

- 672 Achtemeier, G. L., S. A. Goodrick, Y. Q. Liu, F. Garcia-Menendez, Y. T. Hu, and M. T. Odman. Modeling  
673 Smoke Plume-Rise and Dispersion from Southern United States Prescribed Burns with  
674 Daysmoke, *Atmosphere*, 2: 358-88. doi:10.3390/atmos2030358, 2011.
- 675 Aiken, A. C., B. de Foy, C. Wiedinmyer, P. F. DeCarlo, I. M. Ulbrich, M. N. Wehrli, S. Szidat, A. S. H. Prevot,  
676 J. Noda, L. Wacker, R. Volkamer, E. Fortner, J. Wang, A. Laskin, V. Shutthanandan, J. Zheng, R.  
677 Zhang, G. Paredes-Miranda, W. P. Arnott, L. T. Molina, G. Sosa, X. Querol, and J. L. Jimenez.  
678 Mexico city aerosol analysis during MILAGRO using high resolution aerosol mass spectrometry at  
679 the urban supersite (T0) - Part 2: Analysis of the biomass burning contribution and the non-fossil  
680 carbon fraction, *Atmospheric Chemistry and Physics*, 10: 5315-41. doi:10.5194/acp-10-5315-  
681 2010, 2010.
- 682 Alvarado, M. J., C. R. Lonsdale, R. J. Yokelson, S. K. Akagi, H. Coe, J. S. Craven, E. V. Fischer, G. R.  
683 McMeeking, J. H. Seinfeld, T. Soni, J. W. Taylor, D. R. Weise, and C. E. Wold. Investigating the  
684 links between ozone and organic aerosol chemistry in a biomass burning plume from a  
685 prescribed fire in California chaparral, *Atmospheric Chemistry and Physics*, 15: 6667-88.  
686 doi:10.5194/acp-15-6667-2015, 2015.
- 687 Baker, K. R., M. C. Woody, G. S. Tonnesen, W. Hutzell, H. O. T. Pye, M. R. Beaver, G. Pouliot, and T.  
688 Pierce. Contribution of regional-scale fire events to ozone and PM2.5 air quality estimated by  
689 photochemical modeling approaches, *Atmospheric Environment*, 140: 539-54.  
690 doi:10.1016/j.atmosenv.2016.06.032, 2016.
- 691 Carlton, A. G., P. V. Bhave, S. L. Napelenok, E. D. Edney, G. Sarwar, R. W. Pinder, G. A. Pouliot, and M.  
692 Houyoux. Model Representation of Secondary Organic Aerosol in CMAQv4.7, *Environmental  
693 Science & Technology*, 44: 8553-60. doi:10.1021/es100636q, 2010.
- 694 Chai, T., H. C. Kim, P. Lee, D. Tong, L. Pan, Y. Tang, J. Huang, J. McQueen, M. Tsidulko, and I. Stajner.  
695 Evaluation of the United States National Air Quality Forecast Capability experimental real-time  
696 predictions in 2010 using Air Quality System ozone and NO2 measurements, *Geoscientific Model  
697 Development*, 6: 1831-50. doi:10.5194/gmd-6-1831-2013, 2013.
- 698 Davis, A. Y., R. Ottmar, Y. Q. Liu, S. Goodrick, G. Achtemeier, B. Gullett, J. Aurell, W. Stevens, R.  
699 Greenwald, Y. T. Hu, A. Russell, J. K. Hiers, and M. T. Odman. Fire emission uncertainties and  
700 their effect on smoke dispersion predictions: a case study at Eglin Air Force Base, Florida, USA,  
701 *International Journal of Wildland Fire*, 24: 276-85. doi:10.1071/wf13071, 2015.
- 702 de Gouw, J. A., C. Warneke, D. D. Parrish, J. S. Holloway, M. Trainer, and F. C. Fehsenfeld. Emission  
703 sources and ocean uptake of acetonitrile (CH3CN) in the atmosphere, *Journal of Geophysical  
704 Research-Atmospheres*, 108. doi:10.1029/2002jd002897, 2003.
- 705 DeBell, L. J., R. W. Talbot, J. E. Dibb, J. W. Munger, E. V. Fischer, and S. E. Frolking. A major regional air  
706 pollution event in the northeastern United States caused by extensive forest fires in Quebec,  
707 Canada, *Journal of Geophysical Research-Atmospheres*, 109. doi:10.1029/2004jd004840, 2004.
- 708 Delfino, R. J., S. Brummel, J. Wu, H. Stern, B. Ostro, M. Lipsett, A. Winer, D. H. Street, L. Zhang, T. Tjoa,  
709 and D. L. Gillen. The relationship of respiratory and cardiovascular hospital admissions to the  
710 southern California wildfires of 2003, *Occupational and Environmental Medicine*, 66: 189-97.  
711 doi:10.1136/oem.2008.041376, 2009.
- 712 Draxier, R. R., and G. D. Hess. An overview of the HYSPLIT\_4 modelling system for trajectories, dispersion  
713 and deposition, *Australian Meteorological Magazine*, 47: 295-308. 1998.
- 714 Dreessen, J., J. Sullivan, and R. Delgado. Observations and impacts of transported Canadian wildfire  
715 smoke on ozone and aerosol air quality in the Maryland region on June 9-12, 2015, *Journal of  
716 the Air & Waste Management Association*, 66: 842-62. doi:10.1080/10962247.2016.1161674,  
717 2016.



- 718 Drury, S. A., N. Larkin, T. T. Strand, S. M. Huang, S. J. Strenfel, E. M. Banwell, T. E. O'Brien, and S. M.  
719 Raffuse. INTERCOMPARISON OF FIRE SIZE, FUEL LOADING, FUEL CONSUMPTION, AND SMOKE  
720 EMISSIONS ESTIMATES ON THE 2006 TRIPOD FIRE, WASHINGTON, USA, *Fire Ecology*, 10: 56-83.  
721 doi:10.4996/fireecology.1001056, 2014.
- 722 Eatough, D. J., D. A. Eatough, L. Lewis, and E. A. Lewis. Fine particulate chemical composition and light  
723 extinction at Canyonlands National Park using organic particulate material concentrations  
724 obtained with a multisystem, multichannel diffusion denuder sampler, *Journal of Geophysical  
725 Research-Atmospheres*, 101: 19515-31. doi:10.1029/95jd01385, 1996.
- 726 Erbrink, H. J. PLUME RISE IN DIFFERENT ATMOSPHERES - A PRACTICAL SCHEME AND SOME  
727 COMPARISONS WITH LIDAR MEASUREMENTS, *Atmospheric Environment*, 28: 3625-36.  
728 doi:10.1016/1352-2310(94)00197-s, 1994.
- 729 Giglio, L., J. Descloitres, C. O. Justice, and Y. J. Kaufman. An enhanced contextual fire detection algorithm  
730 for MODIS, *Remote Sensing of Environment*, 87: 273-82. doi:10.1016/s0034-4257(03)00184-6,  
731 2003.
- 732 Hamm, S., and P. Warneck. THE INTERHEMISPHERIC DISTRIBUTION AND THE BUDGET OF ACETONITRILE  
733 IN THE TROPOSPHERE, *Journal of Geophysical Research-Atmospheres*, 95: 20593-606.  
734 doi:10.1029/JD095iD12p20593, 1990.
- 735 Hardy, C. C., and C. E. Hardy. Fire danger rating in the United States of America: an evolution since 1916,  
736 *International Journal of Wildland Fire*, 16: 217-31. doi:10.1071/wf06076, 2007.
- 737 Herron-Thorpe, F. L., G. H. Mount, L. K. Emmons, B. K. Lamb, D. A. Jaffe, N. L. Wigder, S. H. Chung, R.  
738 Zhang, M. D. Woelfle, and J. K. Vaughan. Air quality simulations of wildfires in the Pacific  
739 Northwest evaluated with surface and satellite observations during the summers of 2007 and  
740 2008, *Atmospheric Chemistry and Physics*, 14: 12533-51. doi:10.5194/acp-14-12533-2014, 2014.
- 741 Holzinger, R., C. Warneke, A. Hansel, A. Jordan, W. Lindinger, D. H. Scharffe, G. Schade, and P. J. Crutzen.  
742 Biomass burning as a source of formaldehyde, acetaldehyde, methanol, acetone, acetonitrile,  
743 and hydrogen cyanide, *Geophysical Research Letters*, 26: 1161-64. doi:10.1029/1999gl900156,  
744 1999.
- 745 Hu, X. F., C. Yu, D. Tian, M. Ruminski, K. Robertson, L. A. Waller, and Y. Liu. Comparison of the Hazard  
746 Mapping System (HMS) fire product to ground-based fire records in Georgia, USA, *Journal of  
747 Geophysical Research-Atmospheres*, 121: 2901-10. doi:10.1002/2015jd024448, 2016.
- 748 Huang, J., J. McQueen, J. Wilczak, I. Djalalova, I. Stajner, P. Shafran, D. Allured, P. Lee, L. Pan, D. Tong, H.  
749 Huang, G. DiMego, S. Upadhyay, and L. Monache. Improving NOAA NAQFC PM2.5 predictions  
750 with a bias correction approach, *Wea. Forecasting*. doi:10.1175/WAF-D-16-0118.1, 2016.
- 751 Jaffe, D. A., N. Wigder, N. Downey, G. Pfister, A. Boynard, and S. B. Reid. Impact of Wildfires on Ozone  
752 Exceptional Events in the Western US, *Environmental Science & Technology*, 47: 11065-72.  
753 doi:10.1021/es402164f, 2013.
- 754 Johnston, F. H., S. B. Henderson, Y. Chen, J. T. Randerson, M. Marlier, R. S. DeFries, P. Kinney, Dmjs  
755 Bowman, and M. Brauer. Estimated Global Mortality Attributable to Smoke from Landscape  
756 Fires, *Environmental Health Perspectives*, 120: 695-701. doi:10.1289/ehp.1104422, 2012.
- 757 Justice, C. O., L. Giglio, S. Korontzi, J. Owens, J. T. Morissette, D. Roy, J. Descloitres, S. Alleaume, F.  
758 Petitcolin, and Y. Kaufman. The MODIS fire products, *Remote Sensing of Environment*, 83: 244-  
759 62. doi:10.1016/s0034-4257(02)00076-7, 2002.
- 760 Knorr, W., V. Lehsten, and A. Arneth. Determinants and predictability of global wildfire emissions,  
761 *Atmospheric Chemistry and Physics*, 12: 6845-61. doi:10.5194/acp-12-6845-2012, 2012.
- 762 Larkin, N. K., S. M. O'Neill, R. Solomon, S. Raffuse, T. Strand, D. C. Sullivan, C. Krull, M. Rorig, J. L.  
763 Peterson, and S. A. Ferguson. The BlueSky smoke modeling framework, *International Journal of  
764 Wildland Fire*, 18: 906-20. doi:10.1071/wf07086, 2009.



- 765 Lee, Pius, Jeffery McQueen, Ivanka Stajner, Jianping Huang, Li Pan, Daniel Tong, Hyuncheol Kim, Youhua  
766 Tang, Shobha Kondragunta, and Mark Ruminski. NAQFC developmental forecast guidance for  
767 fine particulate matter (PM<sub>2.5</sub>), *Weather and Forecasting*, 32: 343-60. doi:10.1175/waf-d-15-  
768 0163.1, 2017.
- 769 Li, Z., S. Nadon, and J. Cihlar. Satellite-based detection of Canadian boreal forest fires: development and  
770 application of the algorithm, *International Journal of Remote Sensing*, 21: 3057-69.  
771 doi:10.1080/01431160050144956, 2000.
- 772 Malm, W. C., B. A. Schichtel, M. L. Pitchford, L. L. Ashbaugh, and R. A. Eldred. Spatial and monthly trends  
773 in speciated fine particle concentration in the United States, *Journal of Geophysical Research-  
774 Atmospheres*, 109. doi:10.1029/2003jd003739, 2004.
- 775 Neuman, J. A., M. Trainer, S. S. Brown, K. E. Min, J. B. Nowak, D. D. Parrish, J. Peischl, I. B. Pollack, J. M.  
776 Roberts, T. B. Ryerson, and P. R. Veres. HONO emission and production determined from  
777 airborne measurements over the Southeast US, *Journal of Geophysical Research-Atmospheres*,  
778 121: 9237-50. doi:10.1002/2016jd025197, 2016.
- 779 Pan, L., D. Tong, P. Lee, H. C. Kim, and T. F. Chai. Assessment of NO<sub>x</sub> and O<sub>3</sub> forecasting performances  
780 in the US National Air Quality Forecasting Capability before and after the 2012 major emissions  
781 updates, *Atmospheric Environment*, 95: 610-19. doi:10.1016/j.atmosenv.2014.06.020, 2014.
- 782 Pavlovic, R., J. Chen, K. Anderson, M. D. Moran, P. A. Beaulieu, D. Davignon, and S. Cousineau. The  
783 FireWork air quality forecast system with near-real-time biomass burning emissions: Recent  
784 developments and evaluation of performance for the 2015 North American wildfire season,  
785 *Journal of the Air & Waste Management Association*, 66: 819-41.  
786 doi:10.1080/10962247.2016.1158214, 2016.
- 787 Prados, A. I., S. Kondragunta, P. Ciren, and K. R. Knapp. GOES Aerosol/Smoke product (GASP) over North  
788 America: Comparisons to AERONET and MODIS observations, *Journal of Geophysical Research-  
789 Atmospheres*, 112. doi:10.1029/2006jd007968, 2007.
- 790 Prins, E. M., and W. P. Menzel. GEOSTATIONARY SATELLITE DETECTION OF BIOMASS BURNING IN  
791 SOUTH-AMERICA, *International Journal of Remote Sensing*, 13: 2783-99. 1992.
- 792 Rappold, A. G., S. L. Stone, W. E. Cascio, L. M. Neas, V. J. Kilaru, M. S. Carraway, J. J. Szykman, A. Ising, W.  
793 E. Cleve, J. T. Meredith, H. Vaughan-Batten, L. Deyneka, and R. B. Devlin. Peat Bog Wildfire  
794 Smoke Exposure in Rural North Carolina Is Associated with Cardiopulmonary Emergency  
795 Department Visits Assessed through Syndromic Surveillance, *Environmental Health Perspectives*,  
796 119: 1415-20. doi:10.1289/ehp.1003206, 2011.
- 797 Reid, J. S., R. Koppmann, T. F. Eck, and D. P. Eleuterio. A review of biomass burning emissions part II:  
798 intensive physical properties of biomass burning particles, *Atmospheric Chemistry and Physics*,  
799 5: 799-825. 2005.
- 800 Rolph, G. D., R. R. Draxler, A. F. Stein, A. Taylor, M. G. Ruminski, S. Kondragunta, J. Zeng, H. C. Huang, G.  
801 Manikin, J. T. McQueen, and P. M. Davidson. Description and Verification of the NOAA Smoke  
802 Forecasting System: The 2007 Fire Season, *Weather and Forecasting*, 24: 361-78.  
803 doi:10.1175/2008waf2222165.1, 2009.
- 804 Ruminski, M., and S. Kondragunta. Monitoring fire and smoke emissions with the hazard mapping  
805 system - art. no. 64120B. in F. Kogan, S. Habib, V. S. Hegde and M. Matsuoka (eds.), *Disaster  
806 Forewarning Diagnostic Methods and Management*. 2006.
- 807 Ruminski, M., J. Simko, J. Kibler, S. Kondragunta, R. Draxler, P. Davidson, and P. Li. Use of multiple  
808 satellite sensors in NOAA's operational near real-time fire and smoke detection and  
809 characterization program. in W. M. Hao (ed.), *Remote Sensing of Fire: Science and Application*.  
810 2008.
- 811 Saide, P. E., D. A. Peterson, A. da Silva, B. Anderson, L. D. Ziemba, G. Diskin, G. Sachse, J. Hair, C. Butler,  
812 M. Fenn, J. L. Jimenez, P. Campuzano-Jost, A. E. Perring, J. P. Schwarz, M. Z. Markovic, P. Russell,



- 813 J. Redemann, Y. Shinozuka, D. G. Streets, F. Yan, J. Dibb, R. Yokelson, O. B. Toon, E. Hyer, and G.  
814 R. Carmichael. Revealing important nocturnal and day-to-day variations in fire smoke emissions  
815 through a multiplatform inversion, *Geophysical Research Letters*, 42: 3609-18.  
816 doi:10.1002/2015gl063737, 2015.
- 817 Sandberg, D.V., and J. Peterson. A source strength model for prescribed fires in coniferous logging slash,  
818 *1984 annual meeting, Air Pollution Control Association, Northwest Section. 14p.* 1984.
- 819 Sapkota, A., J. M. Symons, J. Kleissl, L. Wang, M. B. Parlange, J. Ondov, P. N. Breyse, G. B. Diette, P. A.  
820 Eggleston, and T. J. Buckley. Impact of the 2002 Canadian forest fires on particulate matter air  
821 quality in Baltimore City, *Environmental Science & Technology*, 39: 24-32.  
822 doi:10.1021/es035311z, 2005.
- 823 Schroeder, W., M. Ruminski, I. Csiszar, L. Giglio, E. Prins, C. Schmidt, and J. Morissette. Validation analyses  
824 of an operational fire monitoring product: The Hazard Mapping System, *International Journal of*  
825 *Remote Sensing*, 29: 6059-66. doi:10.1080/01431160802235845, 2008.
- 826 Singh, H. B., C. Cai, A. Kaduwela, A. Weinheimer, and A. Wisthaler. Interactions of fire emissions and  
827 urban pollution over California: Ozone formation and air quality simulations, *Atmospheric*  
828 *Environment*, 56: 45-51. doi:10.1016/j.atmosenv.2012.03.046, 2012.
- 829 Singh, H. B., L. Salas, D. Herlth, R. Kolyer, E. Czech, W. Viezee, Q. Li, D. J. Jacob, D. Blake, G. Sachse, C. N.  
830 Harward, H. Fuelberg, C. M. Kiley, Y. Zhao, and Y. Kondo. In situ measurements of HCN and  
831 CH<sub>3</sub>CN over the Pacific Ocean: Sources, sinks, and budgets, *Journal of Geophysical Research-*  
832 *Atmospheres*, 108. doi:10.1029/2002jd003006, 2003.
- 833 Sofiev, M., T. Ermakova, and R. Vankevich. Evaluation of the smoke-injection height from wild-land fires  
834 using remote-sensing data, *Atmospheric Chemistry and Physics*, 12: 1995-2006.  
835 doi:10.5194/acp-12-1995-2012, 2012.
- 836 Strand, T. M., N. Larkin, K. J. Craig, S. Raffuse, D. Sullivan, R. Solomon, M. Rorig, N. Wheeler, and D.  
837 Pryden. Analyses of BlueSky Gateway PM<sub>2.5</sub> predictions during the 2007 southern and 2008  
838 northern California fires, *Journal of Geophysical Research-Atmospheres*, 117.  
839 doi:10.1029/2012jd017627, 2012.
- 840 Urbanski, S., V. Kovalev, A. Petkov, A. Scalise, C. Wold, and W. M. Hao. Validation of smoke plume rise  
841 models using ground-based lidar. in C. M. U. Neale and A. Maltese (eds.), *Remote Sensing for*  
842 *Agriculture, Ecosystems, and Hydrology XVI.* 2014.
- 843 Warneke, C., M. Trainer, J. A. de Gouw, D. D. Parrish, D. W. Fahey, A. R. Ravishankara, A. M.  
844 Middlebrook, C. A. Brock, J. M. Roberts, S. S. Brown, J. A. Neuman, B. M. Lerner, D. Lack, D. Law,  
845 G. Hubler, I. Pollack, S. Sjostedt, T. B. Ryerson, J. B. Gilman, J. Liao, J. Holloway, J. Peischl, J. B.  
846 Nowak, K. C. Aikin, K. E. Min, R. A. Washenfelder, M. G. Graus, M. Richardson, M. Z. Markovic, N.  
847 L. Wagner, A. Welti, P. R. Veres, P. Edwards, J. P. Schwarz, T. Gordon, W. P. Dube, S. A. McKeen,  
848 J. Brioude, R. Ahmadov, A. Bougiatioti, J. J. Lin, A. Nenes, G. M. Wolfe, T. F. Hanisco, B. H. Lee, F.  
849 D. Lopez-Hilfiker, J. A. Thornton, F. N. Keutsch, J. Kaiser, J. Q. Mao, and C. D. Hatch.  
850 Instrumentation and measurement strategy for the NOAA SENEX aircraft campaign as part of  
851 the Southeast Atmosphere Study 2013, *Atmospheric Measurement Techniques*, 9: 3063-93.  
852 doi:10.5194/amt-9-3063-2016, 2016.
- 853 Wiedinmyer, C., S. K. Akagi, R. J. Yokelson, L. K. Emmons, J. A. Al-Saadi, J. J. Orlando, and A. J. Soja. The  
854 Fire INventory from NCAR (FINN): a high resolution global model to estimate the emissions from  
855 open burning, *Geoscientific Model Development*, 4: 625-41. doi:10.5194/gmd-4-625-2011, 2011.
- 856 Wiedinmyer, C., B. Quayle, C. Geron, A. Belote, D. McKenzie, X. Y. Zhang, S. O'Neill, and K. K. Wynne.  
857 Estimating emissions from fires in North America for air quality modeling, *Atmospheric*  
858 *Environment*, 40: 3419-32. doi:10.1016/j.atmosenv.2006.02.010, 2006.
- 859 Wotawa, G., and M. Trainer. The influence of Canadian forest fires on pollutant concentrations in the  
860 United States, *Science*, 288: 324-28. doi:10.1126/science.288.5464.324, 2000.



- 861 Xu, L., A. M. Middlebrook, J. Liao, J. A. de Gouw, H. Y. Guo, R. J. Weber, A. Nenes, F. D. Lopez-Hilfiker, B.  
862 H. Lee, J. A. Thornton, C. A. Brock, J. A. Neuman, J. B. Nowak, I. B. Pollack, A. Welti, M. Graus, C.  
863 Warneke, and N. L. Ng. Enhanced formation of isoprene-derived organic aerosol in sulfur-rich  
864 power plant plumes during Southeast Nexus, *Journal of Geophysical Research-Atmospheres*,  
865 121: 11137-53. doi:10.1002/2016jd025156, 2016.
- 866 Yarwood, G., S. Rao, M. Yocke, and G. Whitten. Updates to the Carbon Bond Chemical Mechanism:  
867 CB05, *Technical Report RT-0400675 ENVIRON International Corporation Novato, CA, USA*. 2005.
- 868 Zhang, X. Y., S. Kondragunta, and B. Quayle. Estimation of Biomass Burned Areas Using Multiple-  
869 Satellite-Observed Active Fires, *IEEE Transactions on Geoscience and Remote Sensing*, 49: 4469-  
870 82. doi:10.1109/tgrs.2011.2149535, 2011.

871